UNIVERSITY OF CALIFORNIA,
IRVINE

# Fabrication of Carbon Micro Molds

THESIS

submitted in partial satisfaction of the requirements
for the degree of

MASTER OF SCIENCE

in Mechanical and Aerospace Engineering

by

Rodrigo Martinez Duarte

Thesis Committee:
Professor Marc J. Madou, Chair
Professor Manuel Gamero Castaño
Professor Abraham Phillip Lee

2009

# DEDICATION

A ma chère et tendre épouse, pour la patience et la compréhension dont elle a fait preuve lors de mes longues et laborieuses soirées passées au laboratoire. Ton amour et ton soutien inconditionnels rendent les difficultés de la vie plus faciles à surmonter. Je suis véritablement chanceux de t'avoir dans ma vie

A mis padres Roberto y María del Rosario, mis queridos ‘apa y ‘ama, a mis hermanas Favy y Laris y a mi hermano Rober por siempre apoyarme en todo lo que me he propuesto, echarme porras y trabajar junto conmigo para lograrlo. Gracias por enseñarme a perseverar y a tener fortaleza para adecuarme a los golpes de la vida y por hacerme aprender que el trabajo bien hecho siempre tiene su recompensa. Espero estén tan orgullosos de su Rorri como yo lo estoy de ustedes

Al resto de mi familia, por ser siempre y a toda hora un soporte tan espectacular. Gracias por tantas y tantas cosas que han llenado mi vida de felicidad

A mis amigos, por su alegría y su apoyo. Gracias por escucharme y darme alas en mis proyectos

And last but not least, to God, for blessing me with such beautiful and exciting people

*The pleasure of success strives on maintaining who to share it with*

# TABLE OF CONTENTS


| | Page |
|---|---|
| LIST OF FIGURES | v |
| LIST OF TABLES | vii |
| LIST OF SYMBOLS AND ABBREVIATIONS | viii |
| ACKNOWLEDGEMENTS | x |
| ABSTRACT OF THE THESIS | xi |
| INTRODUCTION | 1 |
| CHAPTER 1. Glass-like Carbon and Carbon MEMS | 8 |
| CHAPTER 2. Fabrication Process I: SU-8 Micro Molds | |
| SU-8 Photoresist | 15 |
| Choice of Substrate | 17 |
| Spin Coat | 18 |
| Soft-Bake | 24 |
| Exposure | 26 |
| Post Exposure Bake | 46 |
| Development and Hard Bake | 47 |
| CHAPTER 3. Fabrication Process II: Carbon Micro Molds and BMG Forming | |
| Carbonization | 50 |
| BMG Thermoplastic Forming | 55 |
| Carbon mold release and Sacrificial molds | 56 |
| CHAPTER 4. Results and Further work | 60 |
| CHAPTER 5. Nanomolding | |
| Electron Beam Lithography | 78 |
| Focused Ion Beam | 79 |
| Nanodroplet Sputtering | 80 |
| Nano Imprint Lithography | 82 |
| CHAPTER 6. Conclusions | 85 |
| REFERENCES | 87 |

# LIST OF FIGURES


| | | Page |
|---|---|---|
| Figure 1 | Basic photolithography steps | 15 |
| Figure 2 | Different film holder designs fabricated in aluminum | 21 |
| Figure 3 | The selected aluminum ring film holder | 22 |
| Figure 4 | Film thickness vs. spin speed for SU-8 2150 under different parameters | 24 |
| Figure 5 | Comparison between the use of transparency and e-beam patterned photomasks | 27 |
| Figure 6 | The *T-topping* effect and its elimination by the use of a SU-8 filter | 28 |
| Figure 7 | Optical pathway between UV lamp and SU-8 film | 30 |
| Figure 8 | Required exposure energy as film thickness varies | 31 |
| Figure 9 | Different wall slopes obtained in positive and negative photoresists without and with back-exposure | 34 |
| Figure 10 | The fabrication of holding substrates and SU-8 patterns with a two-layer process | 36 |
| Figure 11 | Fabrication process for one-layer multi-exposure Grayscale Lithography | 39 |
| Figure 12 | Surface roughness diminishes as exposure dose increases | 41 |
| Figure 13 | Substrate layer thickens as exposure dose increases | 42 |
| Figure 14 | Examples of Grayscale Lithography on SU-8 obtained with the SF-100 system and the mask used to fabricate them | 44 |
| Figure 15 | Correlation between RGB values and resultant SU-8 thickness | 45 |
| Figure 16 | Free standing SU-8 micro molds | 49 |
| Figure 17 | Curved carbon molds derived from SU-8 patterns on a Kapton® film substrate | 54 |

| | | |
|---|---|---|
| Figure 18 | Carbon molds derived from patterned SU-8 on a Cirlex® substrate | 54 |
| Figure 19 | Carbon residues on the BMG wall | 57 |
| Figure 20 | Fine features replication on BMG parts | 58 |
| Figure 21 | Negative and Positive slopes on fabricated molds | 59 |
| Figure 22 | Fabrication sequence for carbon-on silicon molds | 61 |
| Figure 23 | Other carbon-on-silicon geometries | 62 |
| Figure 24 | Achieved 2 μm gaps between BMG structures | 62 |
| Figure 25 | SU-8 structures deformation due to thermal stresses when employing different substrates | 65 |
| Figure 26 | BMG forming process using carbon molds derived from free standing SU-8 | 67 |
| Figure 27 | Carbon molds with minimal surface roughness | 68 |
| Figure 28 | Suggested manufacturing line for the fabrication of carbon molds | 73 |
| Figure 29 | A two-source illumination system for Grayscale Lithography using sequential or a grayscale mask | 76 |

# LIST OF TABLES


| | | Page |
|---|---|---|
| Table 1 | Properties of materials used as substrates compared to those of SU-8 | 18 |
| Table 2 | Spin coating parameters followed by this work | 23 |
| Table 3 | Transmission and Absorption percentage for PET and filter | 30 |
| Table 4 | Advantages and disadvantages of different substrates | 37 |
| Table 5 | Results of attempted carbon etching with different wet chemicals | 56 |
| Table 6 | Fabrication process and time duration of each step | 71 |
| Table 7 | Suggested fabrication process and time duration of each step | 77 |

# LIST OF SYMBOLS AND ABBREVIATIONS

| *Units* | | *Materials and Chemicals* | |
|---|---|---|---|
| °C | Degrees Celsius | Al | aluminum |
| K | Kelvin | Au | gold |
| mm | millimeter | Ni | nickel |
| μm | micrometer | Si | silicon |
| nm | nanometer | | |
| $cm^2$ | centimeter square | BMG | Bulk Metallic Glass |
| $cm^3$ | centimeter cube | PDMS | poly (dimethyl siloxane) |
| h | hour | PET | polyester (Mylar®) |
| min | minute | PI | polyimide |
| s | seconds | | |
| g | gram | GBL | gamma-butyrolactone |
| Da | Dalton | $HNO_3$ | nitric acid |
| W | watt | $H_2SO_4$ | sulfuric acid |
| J | joule | $H_3PO_4$ | phosphoric acid |
| GPa | Gigapascal | HCl | hydrochloric acid |
| mT | millitorr | NaOH | sodium hydroxide |
| sccm | standard cubic centimeters per minute | | |
| cSt | centistokes | | |

*Processes and Techniques*

| | |
|---|---|
| C-MEMS | Carbon MEMS |
| CNC | computer numerical control |
| DRIE | deep reactive ion etching |
| EBL | electron beam lithography |
| ECM | electrochemical machining |
| EDM | electro discharge machining |
| FIB | focused ion beam |
| ICP | inductive conductive plasma |
| LIGA | From the German LIthographie, Galvanoformung, Abformung |
| MEMS | Microelectromechanical Systems |
| NGL | next generation lithographies |
| NIL | nanoimprint lithography |
| PPF | pyrolyzed photoresist films |
| RIE | reactive ion etching |
| SCLR | super cooled liquid region |
| SEM | Scanning Electron Microscope |
| TPF | thermoplastic forming |

*Institutions*

| | |
|---|---|
| IBM | International Business Machines Corporation |
| OSU | Ohio State University |
| UCI | University of California, Irvine |

*Other*

| | |
|---|---|
| CTE | coefficient of thermal expansion |
| RPM | revolutions per minute |
| Tg | glass transition temperature |
| UV | ultra violet |

# ACKNOWLEDGEMENTS

I would like to thank my advisor, Prof. Marc Madou, for giving me the opportunity to conduct exciting research and providing me with so many other opportunities for development in my research career. I hardly imagined graduate school would take me to so many exciting places. His optimism and enthusiasm for so many “crazy” things are worth to follow.

Thanks to my committee members, Prof. Abe Lee and Prof. Manuel Gamero-Castaño, for their enthusiasm on my research and providing kind directions to the next step.

In addition, I would like to thank Prof. Jan Schroers and Dr. Golden Kumar at Yale University for their expertise and collaboration in the forming of Bulk Metallic Glasses.

Most importantly, I want to thank my colleagues and advisors for helping me advance in my scientific pathway and sharing with me the ups and downs of this often frustrating road. There is no price on the support and cheers given after a failed experiment which let us get up and continue with our research. After all, the joy of an achieved result is definitely worth it.

# ABSTRACT OF THE THESIS

Fabrication of Carbon Micro Molds

By

Rodrigo Martinez Duarte

Master of Science in Mechanical and Aerospace Engineering

University of California, Irvine, 2009

Professor Marc J. Madou, Chair

This thesis proposes the use of novel carbon molds for micro molding applications. In contrast to the traditional metal micro molds, the proposed technique derives glass-like carbon micro molds from SU-8 precursors. SU-8 is an epoxy-based negative photoresist that is amenable for the fabrication of very high aspect ratio structures. The developed method is based on traditional UV photolithography but incorporates key enhancements to improve wall verticality and surface roughness and to achieve free standing parts. Grayscale lithography was also employed to fabricate multi-level topographies. The fabricated SU-8 parts are then employed as precursors for the derivation of glass-like carbon through pyrolysis, or thermal degradation, following the Carbon MEMS (C-MEMS) technique. The resultant carbon molds overcomply with the mechanical and thermal integrity of a permanent mold and yet are fabricated at a cost that enables their potential use as sacrificial molds. The developed fabrication process consists of two steps: photolithography and pyrolysis, and does not employ electroplating. Micro molding was demonstrated by the thermoplastic forming of amorphous metals, or bulk metallic glasses, into high aspect ratio micro gears and other geometries. Several

improvements are suggested to reduce fabrication times and costs and to make this process more amenable to have an impact on current micro molding processes. Different approaches to carbon nano molding such as electron beam lithography, focused ion beam, nanodroplet sputtering and nano imprint lithography are also detailed.

# INTRODUCTION

Molding is a fabrication technique with a huge impact on society. Molded parts can now be found in every aspect of our daily lives; from mobile phones, computers and domestic appliances to medical devices such as catheters and implants. The market for molded parts is estimated to be in the order of billions of dollars with plastic molding taking the biggest share of it. In its basic form, molding consists on the filling of a mold with a liquid material for the latter to harden or set with the shape patterned in the mold, and the release of the shaped part, known as a cast, from the mold. This apparently simple process enables the mass production of millions of parts in a very cost-effective way. Casting materials include plastics, glasses, metals, ceramics and a wide variety of alloys. The cost effectiveness of molding resides on the fact that only one, or a few, master molds must be fabricated to generate millions of casts. Even when the fabrication of the master mold might be expensive, depending on the quality, dimensions and complexity required, the cost of an individual cast reduces as the produced volume increases. Therefore, molding is most economically sound when large numbers of a given cast are necessary [1]. Although the basic concept of molding appears trivial, the fabrication of the master mold, the optimization of molding parameters (temperature and pressure for example) and the release of the cast from the mold have proven to be a challenge. In the case of micro molding, or the molding of micrometer sized parts, the fabrication of the master mold is of most importance [1, 2]. The main difference between macro and micro molding is precisely the need of a micrometer sized mold insert in addition to the molding tool. Apart from the fact that new physics must be obeyed during the micro

molding process, the mold insert must be manufactured with more advanced and precise techniques than the traditional Computer Numerical Control (CNC) machining and must fulfill several further requirements than its macro sized counterparts[3]. Perhaps the most challenging of these requirements is the need of smooth side walls. As the size of the mold shrinks, the surface roughness of its walls starts to match the dimensions of the features themselves and reduces fidelity of the molded part to the intended design [4]. Smooth walls are also desired to avoid friction during molding and demolding. Vertical walls, or at an angle slightly wider than 90° if the design allows it, are desired to prevent mechanical interlock of the cast in the mold and assure a clean demolding step. Nevertheless, the micro mold must preserve its structural integrity if it is intended to be used more than once, *i. e.,* not sacrificial. Rigid materials such as metals or ceramics are preferred over polymers (thermosets, thermoplastics or elastomers) in high-precision micro molding as polymers tend to lose their integrity under certain temperature and pressure conditions. Silicon based materials are often employed for experimental or small volume productions as they offer a rigid mold but its brittleness makes it hard to handle. If a lasting mold is the objective, metals, like Ni[5], or carbide alloys (tungsten or silicon carbide) appear to be the materials of choice [6]. Sacrificial molds might become an option in micro molding as some fabrication techniques, like photolithography, allow for the batch fabrication of molds and the amount of material contained in each of them might be insignificant. In this case the mold must be easily and rapidly dissolved. Undoubtedly, the fabrication of a proper master for micro molding is a challenging topic and different approaches may be followed. Current techniques employed for mold fabrication include direct structuring methods like micro CNC machining, electrical

discharge machining (EDM)[7], laser ablation, electrochemical machining (ECM), deep reactive ion etching (DRIE), wet bulk machining (in the case of silicon), focused ion beam milling or micro powder injection and lithography based techniques such as photolithography[8], X-ray lithography or electron beam combined with electroplating. Good reviews include [3, 9-12] The selection of a fabrication technique depends on the desired dimensions, quality, complexity and durability of the mold as well as on economic constrains and the material to be shaped. In general, the selection of the mold material for micro molding depends on its mechanical properties and its versatility to be shaped. For some materials, like metals, the size of their crystals becomes critical as the dimensions of the mold get reduced.

Despite its lengthy process and initial high cost, the most widely accepted technique to fabricate micro molds is that of LIGA, a German acronym for lithography, electroplating and molding. LIGA makes use of X-ray lithography to derive a polymer mold that is then used as a template in the electroplating of a desired metal, usually Ni. The resultant metal mold has the characteristics of a lasting master mold and can be used to produce large volumes of polymer parts. The main advantage of LIGA is its capability to achieve very high aspect ratio structures thanks to the use of X-ray lithography. Unfortunately, the need of a synchrotron hinders the adoption of LIGA by a larger number of commercial applications. Photolithography of SU-8, a negative photoresist, in combination with electroplating offers an affordable alternative to LIGA and is sometimes referred as “poor man’s LIGA.”

The following thesis proposes an alternative to LIGA for deriving micro molds. In contrast to metal molds, the proposed technique derives glass-like carbon micro molds. The developed method makes use of traditional photolithography to derive high aspect ratio features on SU-8. Enhancements to traditional photolithographic methods were incorporated to improve wall verticality. The SU-8 parts are then employed as precursors for the derivation of glass-like carbon through pyrolysis, or thermal degradation, of the negative photoresist. The technique of deriving carbon from micro-patterned organic resists has been dubbed Carbon MEMS (C-MEMS). The resultant carbon mold complies with the mechanical and thermal integrity of a permanent mold and yet is fabricated at a cost that enables its potential use as sacrificial mold. The mold fabrication process consists of two steps, photolithography and pyrolysis, and does not employ electroplating. Moreover, glass-like carbon has been shown to poses a nearly atomic-flat surface [13] and features a melting temperature above 3200 K.

The use of glass-like carbon molds has been previously demonstrated by researchers at Eastman Kodak in the early 1970s [14, 15], and more recently by Takahashi and colleagues [16-18]. They all employed glass-like carbon structures for the molding of glass lenses albeit following a different approach. Researchers at Eastman Kodak employed a polished glasslike carbon piece while Takahashi *et al.* made use of Focused Ion Beam (FIB) milling to pattern commercially available "glassy" carbon. The approach followed in this thesis fundamentally differs from that of Eastman Kodak in that work presented below targets molds with micro and/or nano patterns. In the other hand, it differs from that of Takahashi *et al.* in its ability to mass produce carbon molds in

contrast to the serial nature of FIB milling. This ability might as well yield carbon molds that are sufficiently low priced to be sacrificial.

Even when glass-like carbon molds can be used to mold a variety of traditional materials, such as glass, thermoplastics, ceramics or metals, the focus is on the molding of a novel material: amorphous metals. Amorphous metals, or Bulk Metallic Glasses (BMGs), refer to a class of metal alloys that exhibit high strength, large elastic strain limit, and high corrosion resistance owing to their amorphous nature. They are isotropic, homogeneous, and free from any crystalline defects down to atomic scales. In contrast to amorphous materials, the grain boundaries in crystalline materials represent a weak point in the structure and limit the minimum feature size that can be patterned. BMGs are therefore excellent candidates for small scale applications including precision surgery tools, watch movement components and even micro- nanomolds for other BMGs, plastics and certain metals. The molding of BMGs offers advantages not achieved with conventional electroplating. The latter suffers from a rather limited menu for material selection and often results in parts with non-uniform deposition at sharp edges and recessed areas, stresses that are very dependent on the electroplating current and non-uniform mechanical properties imposed by the metal grain size. The BMG molding can be carried out using complex alloys which are intrinsically superior in strength, corrosion resistance and wear resistance compared to conventional electroplated metals. BMGs are also free of crystalline defects and as a consequence are homogeneous and isotropic.

It has been shown that the BMGs can be thermoplastically formed like plastics [19, 20]. Thermoplastic forming (TPF) takes place in the supercooled liquid region (SCLR) where the viscosity of BMG drops significantly allowing it to flow under small applied pressure. TPF of BMGs has been used for a wide range of applications including net-shape processing, extrusion, synthesis of amorphous metallic foams and blow molding [21-23]. TPF of BMGs has the potential to become an alternative to current metal forming techniques used in microforming such as electroplating. A first advantage of TPF of BMGs stems from its simplicity compared to electroplating. Secondly, electroplating of metals suffers from a rather limited menu for material selection, and often results in parts with non-uniform deposition at sharp edges and recessed areas, stresses that are very dependent on the electroplating current, and non-uniform mechanical properties imposed by the metal grain size. BMG molding can be carried out using complex alloys which are intrinsically superior in strength, corrosion resistance and wear resistance compared to conventional electroplated metals. BMGs are also free of crystalline defects, which results in homogeneous and isotropic parts. Lastly, even when surface finish of molded BMG parts strongly depends on the surface finish of the mold used, their surface roughness can be reduced by re-heating above their glass transition temperature [24], an improvement not achievable with metal parts fabricated by electroplating. The main limiting factor in the TPF of BMGs is in the type of master molds required to guarantee stability under TPF temperatures (200-450 °C) and pressures (10-30 MPa). Unfortunately, under such conditions inexpensive polymer molds like the ones used for electroplating and LIGA are not an option. However, the proposed glass-like carbon

molds are stable at temperatures exceeding the processing temperatures for TPF of BMGs and have sufficient mechanical strength to be used as master molds for TPF of BMGs.

This thesis begins with an overview on glass-like carbons and C-MEMS in Chapter 1. The outstanding properties of this material are exposed together with a brief history on the derivation of carbon microstructures from organic polymers. Chapter 2 and 3 detail the method developed to fabricate carbon molds and its forms of use. Chapter 2 deals with the derivation of the polymer precursor, in this case SU-8. Chapter 3 treats the mechanisms of pyrolysis, the molding of BMG using carbon molds and the release of the BMG from the mold. Achieved results and relevant discussions are exposed on Chapter 4 along with potential improvements to the general process. At last, Chapter 5 explores alternative technologies to photolithography for the fabrication of nano molds and complex micro molds. Electron-beam Lithography (EBL), Focused Ion Beam (FIB), Nanodroplet Sputtering and Nanoimprint Lithography (NIL) are explored.

# CHAPTER 1. Glass-like Carbon and Carbon MEMS

Glass-like carbons[1] are derived through the carbonization of organic polymers in inert atmospheres (more details on carbonization in Chapter 3). The resultant carbon has a glass-like appearance in the sense that is smooth, shiny and exhibits a conchoidal fracture[2][25]. The properties of the material make it an ideal candidate for mold fabrication. It is impermeable to gases and extremely inert, with a remarkable resistance to chemical attack from strong acids such as nitric, sulfuric, hydrofluoric or chromic and other corrosive agents such as bromine. Even when it does react with oxygen it only does so at high temperatures. Its rates of oxidation in oxygen, carbon dioxide or water vapor are lower than those of any other carbon. X-ray diffraction studies have shown that glass-like carbon presents an extremely small pore size of a closed nature, and that has an amorphous structure [26-33].

Regarding its mechanical properties, glass-like carbon has a hardness of 6 to 7 on Mohs' scale, a value comparable to that of quartz. Its density ranges from 1.4 to 1.5 g/cm$^{-3}$. Glass-like carbon features a coefficient of thermal expansion of 2.2-3.2 X $10^{-6}$/K which

[1] In 1995 the IUPAC (International Union of Pure and Applied Chemistry) defined glass-like carbon as the material derived by the pyrolysis of organic polymers and recommended that the terms "Glassy carbon" and "Vitreous carbon", which had been introduced as trademarks, should not be used as synonymous for glass-like carbon. From a scientific viewpoint, the terms vitreous and glassy suggest a similarity with the structure of silicate glasses which does not exist in glass-like carbon, except for the pseudo-glassy appearance of the surface [103].

[2] Some crystals do not usually break in any particular direction, reflecting roughly equal bond strengths throughout the crystal structure. Breakage in such materials is known as fracture. The term conchoidal is used to describe fracture with smooth, curved surfaces that resemble the interior of a seashell; it is commonly observed in quartz and glass. Conchoidal fracture. (2009). In Encyclopaedia Britannica. Retrieved April 08, 2009, from Encyclopaedia Britannica Online: http://www.britannica.com

compares to that of Si [34] and some BMGs [35]. Its Young Modulus varies between 10 and 40 GPa. Because its thermal conductivity is only 7 W/mK it is considered as thermally inert (compare to 401 W/mK of copper and 1 W/mK of Pyrex® glass). [36-41]. Even when the overall properties of the resulting carbon depend on the nature of the precursor used, they do not change very significantly [42] and the above values could be employed as an initial reference. Up to this date a consensus on the crystalline structure of glass-like carbon has not been reached. The most widely known and accepted model is the one that considers this type of carbon as made up of tangled and wrinkled aromatic ribbon molecules that are randomly cross-linked by carbon-carbon covalent bonds. The ribbon molecules form a networked structure, the unit of which is a stack of high strained aromatic ribbon molecules. Such structure of crystallites reflects the features of thermosetting resins structure which are commonly used as precursors for glass-like carbons. This model explains the most experimental results obtained so far on glass-like carbons including its impermeability, brittleness and conductivity. [41-45]. Other models exist including the "oxygenated Tetrahedral-Graphitic parts" model of Kakinoki [43], the "crumpled sheets" model of Oberlin [33], the "closed pores" model by Shiraishi [46]and the "globular" model by Fedorov [47]. Excellent reviews on the structure of glass-like carbon can be found in [41]and [45].

Glass-like carbon is characterized as a type of char[3] and is classified as a non-graphitizable, or non-graphitizing, carbon. Glass-like carbon does not graphitize

[3] Char is a solid decomposition product of a natural or synthetic organic material. If the precursor has not passed through a fluid stage, char will retain the characteristic shape of the precursor (although becoming of smaller size). For such materials the term "pseudomorphous" has been used. In contrast, coke is

even when heat treated at 3273 K (3000 °C). The inability of the graphitic planes to grow and stack parallel to each other even at high temperatures is due to the entangled nature of glass-like carbon structure. Non-graphitizable carbons are mechanically hard and are sometimes referred as hard carbons[48]. For the sake of clarity, even when the term pyrolytic carbon might suggest a synonym for glass-like carbons, the former term only refers to carbon materials deposited from gaseous hydrocarbon compounds. The term pyrolytic carbon does not describe the large range of carbon materials obtained by thermal degradation (thermolysis, pyrolysis) of organic compounds when they are not formed by chemical vapor deposition. Materials deposited by physical vapor deposition are not covered either by the term pyrolytic carbon.

Glass-like carbon appears to be first derived in 1915 by Weintraub and Miller [49]. However, a sustained flow of publications did not begin until the early 1960s when independent groups from Japan and England first disclosed the properties and methods of derivation of the novel carbon allotrope [36, 37, 50, 51]. Its unique properties have been beneficial to various applications along the years. Initially, its extreme chemical inertness and gas impermeability were exploited to fabricate laboratory equipment such as beakers, basins and boats [38]. Since glass-like carbon is not wetted by a wide range of molten metals, it is an ideal material for the fabrication of crucibles with applications in metallurgical and chemical engineering [37]. Its resistance to erosion and high melting point makes it an ideal material for mandrels, steam, fuel and rocket nozzles and other equipment in mechanical and electrical applications. Moreover, glass-like carbon has

produced by pyrolysis of organic materials that have passed, at least in part, through a liquid or liquid-crystalline state during the carbonization process.

been used in heart valve implants and other biomedical devices thanks to its biocompatibility [52-54] . “Glassy” carbon electrodes have become so popular that they represent a significant fraction of the multi-billion electrochemistry market [55].

From the microfabrication standpoint, glass-like carbon microstructures were not reported until the late 1990s by Schueller and co-workers at Harvard University. In their process, polydimethylsiloxane (PDMS) molds were fabricated using soft lithography and then used to pattern furfuryl alcohol-modified phenolic resins and phenol-formaldehyde resins, which were subsequently carbonized [56-60]. This fabrication technique allowed them to work with flat or curved surfaces and derive different structures (including free-standing lateral comb drives, diffraction gratings and grids) with dimensions as small as a few micrometers and featuring high aspect ratios if desired [60]. Microelectromechanical functions were also demonstrated [57]. By the end of that same decade, initial work on the derivation of carbon from photoresists emerged in the quest for alternatives to carbon films produced by physical deposition techniques. The interest was driven by the use of pyrolyzed photoresists in batteries, electrochemical sensors, capacitors and MicroElectroMechanical Systems (MEMS). Electrochemical studies of carbon films derived from positive photoresists were conducted in 1998 by Kim, Song, Kinoshita, Madou and White in Berkeley, CA [61] and later by Ranganathan, McCreery, Majji and Madou [62] at Ohio State University (OSU). By 2000, Kostecki, Song and Kinoshita patterned these carbon films as microelectrodes and studied the influence of the geometry in their electrochemical response [63]. Pyrolyzed Photoresist Films, or PPF, still derived from positive resists were surface-characterized in 2001 and determined to

have a near-atomic flatness [13]. The resultant carbon showed an electrochemical behavior similar to glass-like carbon although with decreased surface roughness. In 2002 the derivation of carbon from negative photoresists was reported by Singh, Jayaram, Madou and Akbar at OSU. They used SU-8, a relatively new epoxy-based photoresist at the time [64, 65], and polyimide to fabricate circular patterns. The carbon obtained with this precursor showed higher resistivity and vertical shrinkage than the one synthesized from positive resists. Furthermore, the carbon derived from SU-8 showed higher vertical shrinkage and poorer substrate adhesion than that from polyimide. Nevertheless, resistivity from SU-8 carbon was slightly lower than polyimide's [66]. In 2005, structures with aspect ratios higher than 10 were reported by Wang, Jia, Taherabadi and Madou at the University of California, Irvine (UCI). This achievement was possible thanks to the use of a two-step heating process during pyrolysis. This novel process allowed for the release of residual oxygen contained in the polymer structures that had caused the precursor to burn rather than pyrolyze, even in an oxygen-free atmosphere. A variety of complex high-aspect ratio Carbon-MEMS (C-MEMS) structures, such as posts, suspended carbon wires, bridges, plates, self organized bunched posts and networks, were built in this way. The variation in structure shrinkage depending on the original polymer was also reported [67, 68]. For example, structures with thickness below 10 um usually shrink approximately by 90%, while hundreds-of-microns thick features shrink approximately 50%. Also in 2005, the electrical properties and shrinkage behavior of both positive and negative resists after pyrolysis were characterized by Park and co-workers at UCI. They corroborated the decrease in resistivity of glass-like carbons as the pyrolysis final temperature increases. They also demonstrated how the largest

shrinkage takes place below 873 K (600 °C) for all the photoresists tested [69]. Electron beam lithography (EBL) was used in 2006 to fabricate suspended glass-like carbon microstructures [70]. Continuous work on C-MEMS has been conducted since 2004 by the same group at UCI and collaborators in a variety of applications including Lithium-ion batteries[71-74], fuel cells [75, 76], electrochemical sensors[77], cell culturing substrates[78], dielectrophoresis [79-83, 83-86], micromolding [87] and fractal electrodes[88, 89]. Other groups have also recently integrated carbon structures for their use in gas sensors[90].

Carbon-MEMS (or C-MEMS) can be defined as the set of methods that can be used to derive glass-like carbon structures from patterned organic polymers, featuring dimensions ranging from hundreds of micrometers down to tens of nanometers. C-MEMS combines different polymer micro and nanofabrication techniques with pyrolysis or thermal degradation to derive glass-like carbon features. These fabrication techniques include, but are not limited to, stamping, casting, machining and lithography. The choice of each technique, and the organic polymer, is dictated by the quality, complexity and final dimensions of the desired carbon part. The next chapter details a photolithographic process to fabricate SU-8 structures for carbonization. Enhancements to traditional photolithography are incorporated to obtain free standing carbon molds with improved complexity, wall verticality and surface roughness.

# CHAPTER 2. Fabrication Process I: SU-8 Micro Molds

Photolithography refers to patterning with light. The material to be patterned, a photoresist, changes its chemical composition upon being exposed to light with specific wavelengths (usually 365 nm, the i-line, or 436 nm, the g-line). In a positive photoresist, light originates a scission on the polymer chain that renders the exposed part more soluble to certain chemicals, known as developers. In contrast to positive resists, light causes cross-linking in negative resists which makes the shined section less soluble in a developer. At the end, the area of positive resist exposed to light is dissolved away while in the case of a negative resist the exposed area remains. Masks, a patterned stencil that enables the selective pass of light, must then be designed accordingly to the kind of photoresist being used and the desired final topography.

The incorporation of photolithography to the C-MEMS toolbox enables a more precise control on the dimensions and complexity of the precursor polymer structures. The existence of commercial high-quality precursors and standardized photolithography tools make the fabrication process and the dimensional control highly reproducible. Photolithography generally involves a set of basic processing steps: photoresist deposition, soft bake, exposure, post-exposure treatment and developing (Fig. 1). An enhanced photolithography process using SU-8 as photoresist is detailed after a short overview on the properties and uses of SU-8.

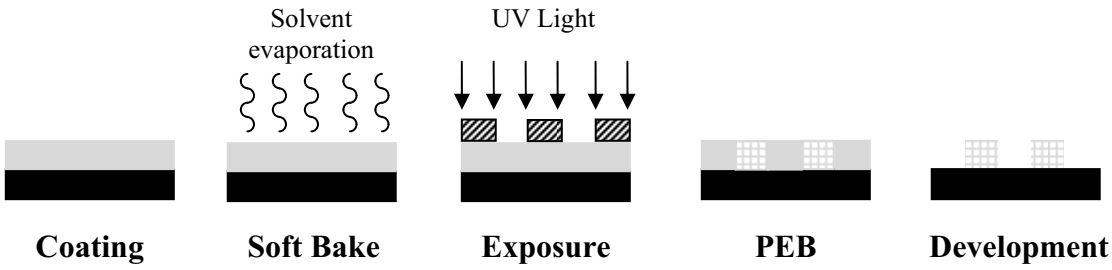


**Figure 1** Basic photolithography steps

*SU-8 Photoresist*

SU-8 is an acid-catalyzed negative photoresist, made by dissolving a Bisphenol A novolac resin (EPON® SU-8 resin, a registered trademark of Shell Chemical Company) in an organic solvent such as cyclopentanone or GBL (gamma-butyloractone) and adding up to 10% in weight of triarylsulfonium hexafluoroantimonate as a photoinitiator. The viscosity and hence the range of thicknesses accessible, is determined by the ratio of solvent to resin. The EPON resist is a multifunctional, highly-branched epoxy derivative that consists of bisphenol-A novolac glycidyl ether. On average, a single molecule contains 8 epoxy groups which explain the 8 in the name SU-8. In a chemically amplified resist like SU-8, one photon produces a photoproduct that in turn causes hundreds of reactions to change the solubility of the film. Since each photolytic reaction results in a "amplification" via catalysis, this concept is dubbed "chemical amplification" [91]. SU-8 photoresist was developed by scientists at IBM who discovered that certain photo-initiators, such as onium salts, polymerize low-cost epoxy resins such as EPON® SU-8. Compositions of SU-8 photoresist were patented by IBM as far back as 1989 [92] and 1992 [93]. Original compositions were intended for printed circuit board and e-beam

lithograpy. SU-8 photoresists became commercially available in 1996 through MicroChem Corporation (Newton, MA). Because of its aromatic functionality and highly cross-linked matrix, the SU-8 resist is thermally stable and chemically very inert. After a hard bake, it withstands nitric acid, acetone, and even NaOH at 90°C. Moreover, it is more resistant to prolonged plasma etching and better suited as a mold for electroplating than Poly(methyl methacrylate) (PMMA) [94]. The low molecular weight [~ 7000 ± (1000) Da] and multifunctional nature of the epoxy gives it the high cross-linking propensity, which also reduces the solvent-induced swelling typically associated with negative resists. As a result, very fine feature resolution, unprecedented for negative resists, can be obtained. Low molecular weight characteristics also translate into high contrast and high solubility. Because of its high solubility very concentrated resist casting formulations can be prepared. The increased concentration benefits thick film deposition (up to 500 μm in one coat) and planarization of extreme topographies. The high epoxy content promotes strong SU-8 adhesion to many types of substrates and makes the material highly sensitive to UV exposure. On the negative side, the thermal mismatch of SU-8 on a Si substrate produces stress and may cause film cracking. Moreover, the absorption spectrum of SU-8 shows much higher absorption coefficients at shorter wavelengths (< 350 nm). As a result lithography using a broadband light source tends to result in over-exposure at the surface of the resist layer. The resulting developed photoresist tends to have a negative slope, or an angle with the substrate narrower than 90°, which is not good for mold applications. The exaggerated negative slope at the top of the resist structure surface is often called *T-topping*. For a recent review on SU-8 and the fabrication of high aspect ratio features the reader is referred to [95]. The employed

SU-8 formulation for this work was MicroChem's SU-8 2150. This formulation features 76.75% Solids, has a viscosity of 80000 cSt and a density of 1.238 g/cm$^3$ [96].

### *Choice of Substrate*

Traditional SU-8 photolithography is usually conducted on rigid substrates such as Silicon, quartz and glass. In these cases the coefficient of thermal expansion (CTE) of the substrate (<10 $10^{-6}$/K) is significantly different from that of SU-8 (50-52 $10^{-6}$/K) resulting in SU-8 patterns with built in stresses that might cause film cracking. A substrate material that matches the CTE of SU-8 is therefore desired. A further requisite for the obtainment of free standing carbon molds is that the substrate material must either get carbonized together with the patterned SU-8 or get separated from the mold before carbonization, for instance peeling the SU-8 patterns from the substrate. Unfortunately, silicon, glass or quartz do not carbonize under a pyrolysis process and provide good adhesion to SU-8. These facts, together with the fact that the substrate is rigid, make it quite challenging to remove the SU-8 pattern in an easy, reliable way. Several different substrates were employed in this work: 4" standard silicon wafers and 4" diameter discs of either Kapton® (127 μm thick), Cirlex® (1.5 mm) or Mylar® (70 μm). Carbon-on-silicon and free standing carbon molds were obtained. Free standing carbon molds were fabricated using polyimide (Kapton® and Cirlex®) as substrate and carbonizing the whole polyimide-SU-8 piece or by using polyester (Mylar®) as a peel-off substrate that gets easily removed from the SU-8 part prior to carbonization. In Chapter 4, Fig. 25 is shown how free standing molds offer better fidelity to the original design than those fabricated on silicon by reducing stresses due to thermal mismatch. The difference between the CTE

of the substrate material and that of SU-8 is of most importance during the carbonization process, where the use of polyimide, or better yet the elimination of the substrate, yields significant better results than the use of silicon. Table 1 shows the relation between the properties of different materials to those of SU-8.

**Table 1** Properties of materials used as substrates compared to those of SU-8

| Material | Coefficient of Thermal Expansion ($10^{-6}$/K) | Thermal Conductivity at 293 K (W/m-K) | Density (g/ $cm^3$) | Glass temperature or melting point |
|---|---|---|---|---|
| **Silicon** [34] | 2.6 – 4.442 | 1.56 | 2.33 | 1414 °C (1687 K) |
| **Polyimide (PI)** [97, 98] | 20 - 40 | 0.120 | 1.42 | 360-410 °C (633 – 683 K) |
| **Polyester (PET)**[99] | 17.1 | 0.37 | 1.390 | 254 °C (527 K) |
| **SU-8** [100] | 50 - 52 | 0.2 | 1.2 | 50-55 °C (323-328 K) not cross-linked >200 °C (>473 K) when cross-linked |

## *Spin Coat*

The most common method to deposit photoresists is spin coating. In this method, centrifugal forces cause the resist to flow to the edges, where it builds up until expelled when its surface tension is exceeded. The resulting polymer thickness is a function of spin speed, solution concentration, and molecular weight (measured by intrinsic viscosity). Generally, the photoresist is dispensed onto the substrate, which is held in place by a vacuum-actuated chuck in a resist spinner [101]. A rotating speed of about 500 RPM is commonly used during the dispensing step to spread the fluid over the substrate. After the dispensing step, it is common to accelerate to a higher speed to thin down the

fluid near to its final desired thickness. Typical spin speeds for this step range from 1500 to 6000 RPM, depending on the properties of the fluid (mostly it viscosity) as well as the substrate. This step can take from a few seconds to several minutes. The combination of spinning speed and time will generally define the final film thickness and its uniformity. An empirical expression to predict the thickness of the spin coated film as a function of its molecular weight and solution concentration is given in [102]. The photoresist film, after being spin coated into the substrate, must have a uniform thickness and be chemically isotropic so that its response to exposure and development is uniform. Film uniformity tends to decrease as the thickness increases.

In order to conduct spin coating the substrate must be rigid enough to keep planar during the process. Of the polymer films used, only Cirlex® fulfilled this requisite. Cirlex® is an adhesive-less stack of polyimide layers that can achieve thicknesses of several hundred micrometers. In this case a 1.5 mm thick Cirlex® sheet was CNC machined into 4" discs and used directly as a substrate. In the case of Kapton® (polyimide or PI) and Mylar® (polyester or PET) films, 127 μm and 70 μm thick respectively, a rigid metal holder had to be engineered and fabricated.

Aluminum was chosen to fabricate the film holder given is low density (2.7 g/cm$^3$), high thermal conductivity (237 W/m-K), similar coefficient of thermal expansion (23.1 $10^{-6}$/K) to polyester (PET) and polyimide (PI), excellent corrosion resistance, easy processing and its relative low cost. Several film holder designs were explored and are shown in Fig. 2 with mounted PET films. Aluminum parts, 4" discs and rings, were CNC machined

from a 1.78 mm thick Al sheet. All of the designs made use of nuts and bolts to secure the film to the substrate. Rubber rings were used to prevent SU-8 from getting into the nut and bolt arrangement thus facilitating their removal during the process (see section on Exposure below). Out of the proposed designs the one consisting of only an aluminum ring was chosen (Fig. 2 middle and Fig. 3). By only employing a ring the overall weight of the holder gets greatly reduced and allows significantly higher spin speeds (>4000 RPM) than those achieved by other designs, namely the ones requiring the aluminum disc. A wider range of spin speeds means more film thickness options given a photoresist composition. The use of the ring design also creates a transparent back window, when using PET as substrate, into the coated SU-8. This window enables the back-exposure of SU-8 which optimizes the wall slope for molding applications (see section on Exposure below). This advantage is only exploited with the use of Ultraviolet (UV) transparent films such as PET. Polyimide cannot be used as it efficiently filters out UV light wavelengths. With the proper stretching and tightening of the film to the aluminum ring a rigid enough substrate is obtained (see Fig. 3).

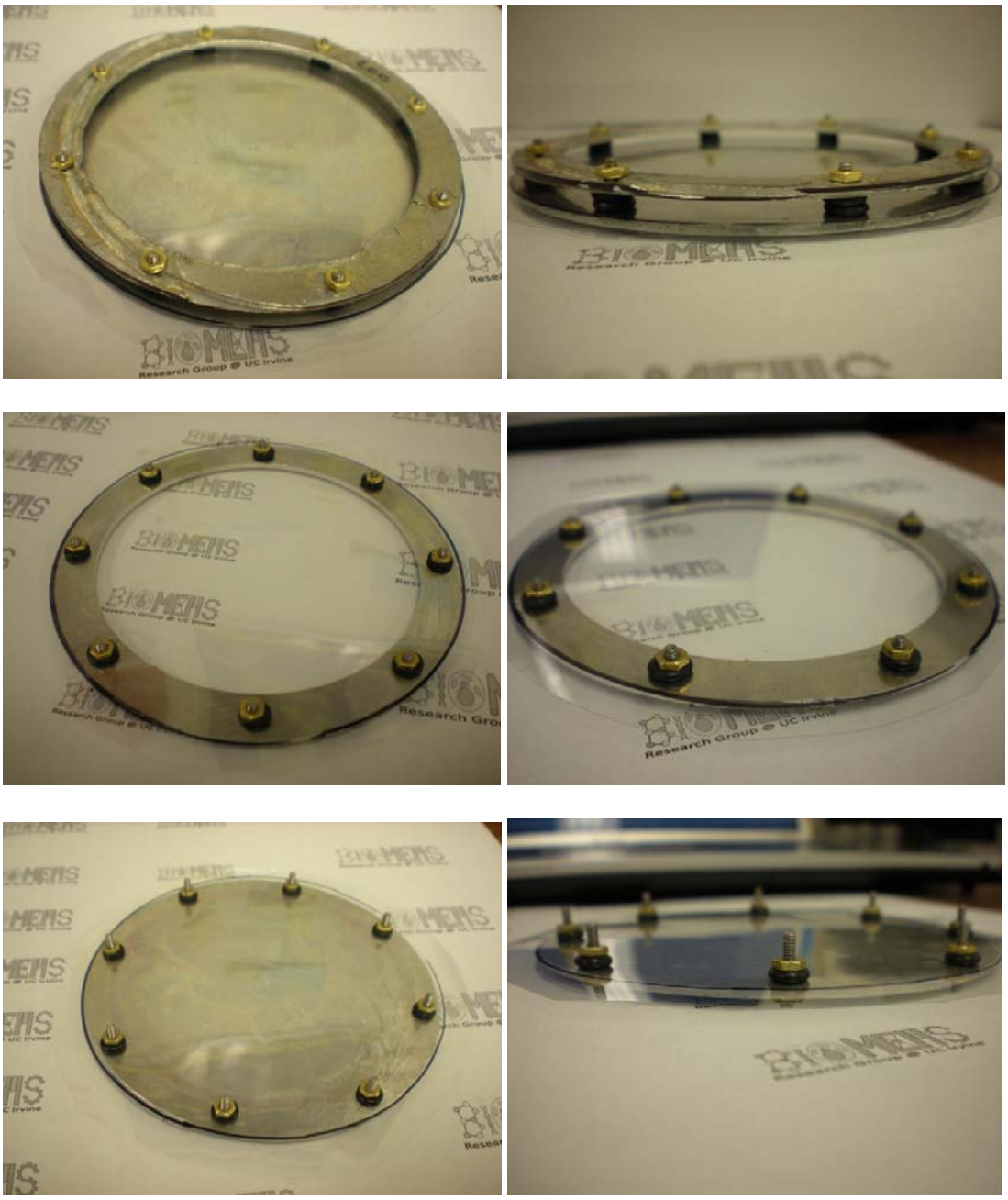

**Figure 2** Different film holder designs fabricated in aluminum

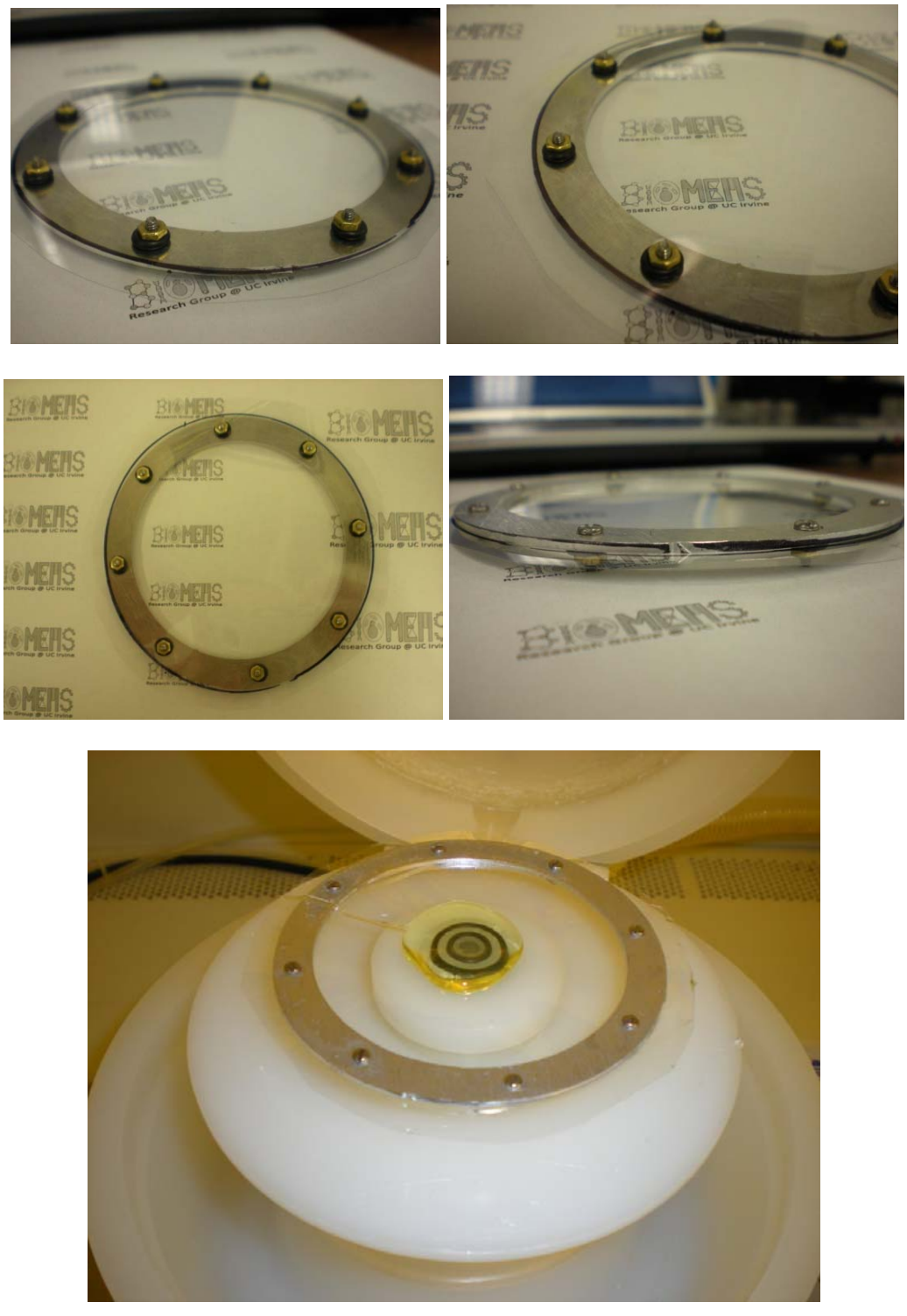

**Figure 3** The selected aluminum ring film holder

Independently of the substrate, the spin coating parameters of SU-8 2150 followed in this work are based on those presented in MicroChem datasheet [96] but introducing a few variants, namely acceleration rates and spinning times. A Laurell spinner model WS-400B-6NPP/LITE (Laurell Technologies, North Wales, PA) was employed. Spin coating was conducted in two steps. The first step was for the uniform spreading of SU-8 over the substrate and was performed following an acceleration ramp to 500 RPM of 340 RPM/s. This spin speed was held for 15 seconds. The second step is for the thinning of the photoresist onto a desired thickness so the final spin speed implemented depends on the desired film thickness. In order to improve film uniformity the duration of this step was increased from the recommended 30 s to 60 s. The acceleration of this step was maintained at 340 RPM/s. A resume of the spin parameters implemented during this work can be found in Table 2. The use of these parameters causes the spin speed vs. film thickness curve presented in SU-8 2150 processing datasheet (thinner line) [96] to shift downwards as shown in Fig. 4 (thicker line).

**Table 2** Spin coating parameters followed by this work

| Step | Spin Speed (RPM) | Time (s) | Acceleration Rate (RPM/s) |
|---|---|---|---|
| 1 | 500 | 15 | 340 |
| 2 | Depends on desired thickness. See Fig. 4 | 60 | 340 |

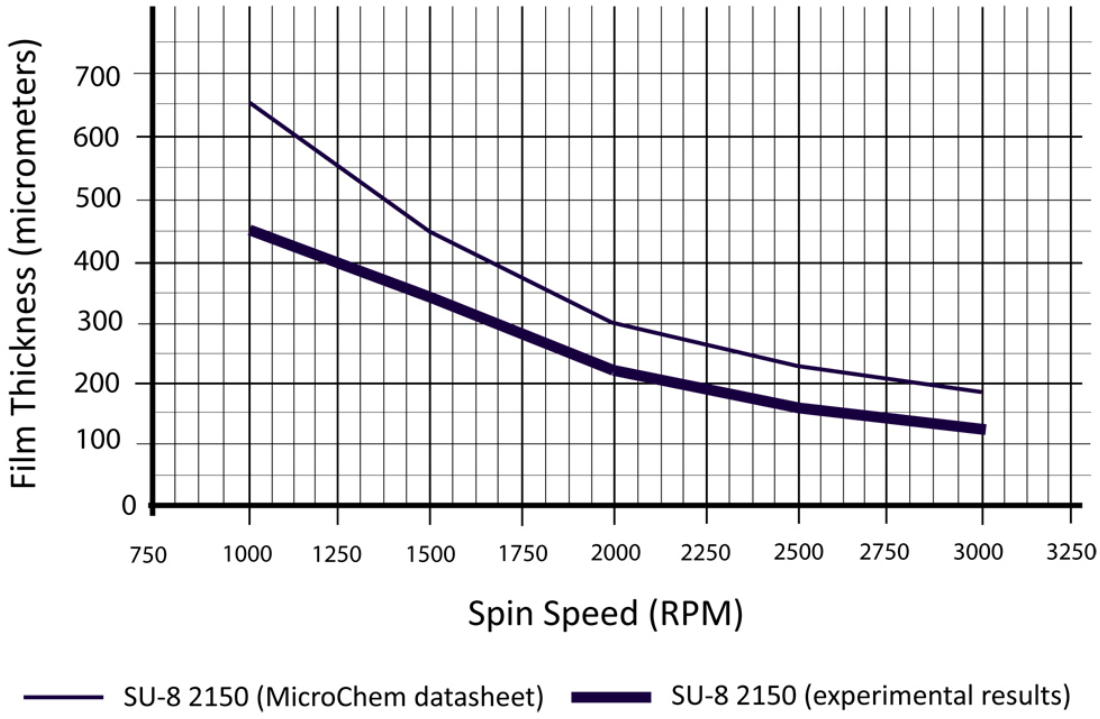


**Figure 4** Film thickness vs. spin speed for SU-8 2150 under different parameters

*Soft-bake*

After SU-8 coating, the substrate-resist arrangement is soft baked (also known as pre-exposure baked or prebaked). The objective of this step is to evaporate the solvent, in this case cyclopentanone (SU-8 2000 series uses cyclopentanone as solvent while SU-8 series uses gamma-butyrolactone, or GBL), still contained in the resist. This is a critical step in that failure to sufficiently remove the solvent affects the resist profile but excessive baking destroys the photoactive compound and reduces sensitivity. Soft bake was conducted at 95 °C, either on a hotplate or in a convection oven, for different times depending on the type of substrate and the film thickness. Hot plating the resist is faster, more controllable, and does not trap solvent like convection oven baking does. In

convection ovens the solvent at the surface of the resist is evaporated first, and this can cause an impermeable resist skin, trapping the remaining solvent inside. However, the thermal conductivity of PET and PI (see Table 1) forces the use of an oven. For those samples where silicon was used as substrate a hot plate was employed. Extended bake times ranging from 2 hours, on a hotplate for film thicknesses of 50-100 μm, to 16 hours, in an oven for >250 μm thick films, were implemented with positive results.

If a proper soft bake was conducted, the resultant resist is free of solvent and does not flow at room temperature. At this point the glass transition temperature, Tg, of the deposited photoresist matches that of pure SU-8 and only re-flows when heated above 55 °C. In the case of PET and PI substrates, the nuts and bolts used to hold the polymer film rigid during spin coating should be removed together with the rubber rings to facilitate the exposure step to be performed next. If the SU-8 and polymer films cool to room temperature attached to the aluminum ring, the SU-8 film hardens and maintains a rigid disk shape. Only at that point is safe to remove the nuts and bolts. Thanks to a small quantity of SU-8 flowing in between the aluminum ring and the polymer film during coating, the film stays “glued” to the aluminum holder even in the absence of the nuts and bolts. This fact represents an advantage in the rest of the process, especially after post exposure baking when it prevents the SU-8 film from curling up due to internal stresses.

*Exposure*

After soft baking, the resist-coated substrates, silicon or polymer, are transferred to an illumination or exposure system where they are aligned with the features on a mask. In the simplest setup, as is the case in this work, an exposure system consists of a UV lamp illuminating the resist-coated substrate through a mask without any lenses between the two. The purpose of the illumination systems is to deliver light with the proper intensity, directionality, spectral characteristics, and uniformity across the substrate, allowing a nearly perfect transfer or printing of the mask image onto the resist in the form of a latent image. The incident light intensity (in $W/cm^2$) multiplied by the exposure time (in seconds) gives the incident energy ($J/cm^2$) or dose across the surface of the resist film. UV radiation induces a chemical reaction in the exposed areas of SU-8 generating acids that initiate the cross-linking of the polymer.

A SUSS MicroTec MA-6/BA6 (Waterbury Center, VT) mask aligner was used for this work. The first major step towards improving surface roughness of the mold walls is to use high quality masks. It is usually the case in research, especially when under economic restraints, to employ transparency masks for photolithography. These kinds of masks are plastic sheets that have been patterned (printed) with a high resolution plotter and can be used directly to pattern photoresists. Even when they are affordable, the quality and resolution that can be achieved with transparency masks are highly dependent on the specifications of the plotter. Maximum resolution of commercially available plotter is currently 7 μm. Higher quality masks are fabricated by patterning a chromium film that has been evaporated on low UV-absorption quartz plates. For ultimate quality, patterning

is done with an electron beam tool. As expected, the obtained results are significantly better than those achieved with transparency masks (See Fig. 5). The use of chromium-on-quartz photomasks patterned with e-beam yields walls with minimal roughness.

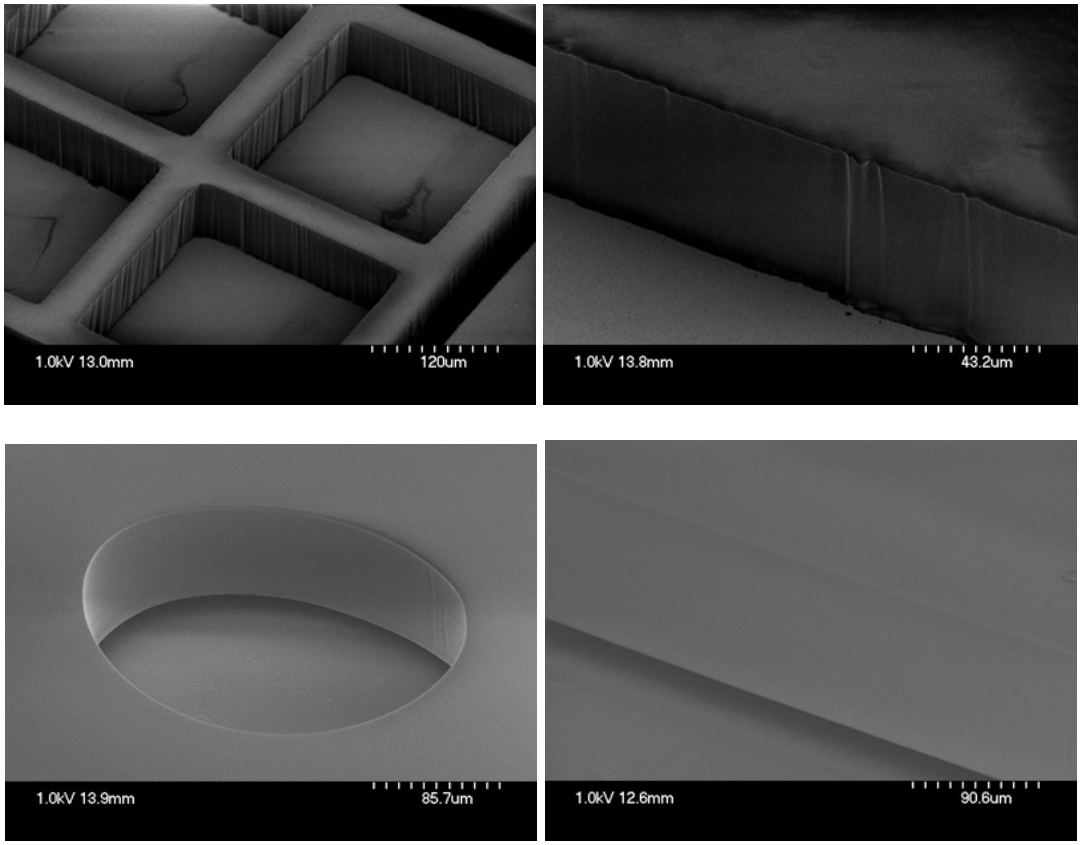


**Figure 5** Comparison between the use of transparency (top) and e-beam patterned photomasks (bottom)

The effect of *T-topping* has been mentioned before as an effect that negatively impact photoresists such as SU-8, especially when deriving high aspect ratio structures. The reason behind *T-topping* is the fact that SU-8 strongly absorbs light wavelengths that are less than 350 nm. If using a broadband light source for exposure, as it is usually the case,

UV light shorter than 350 nm is strongly absorbed near the surface creating locally more acid that diffuses sideways along the top surface. Selective filtration of the light source is then required to eliminate these undesirable shorter wavelengths. An easy and affordable way to implement a filter is by using a 50-100 μm layer of SU-8 placed in between the light source and the mask. Commercial high pass filters with cut-out wavelength of 360 nm are also available. This work made use of the SU-8 layer approach. *T-topping* was immediately eliminated with the use of a 50 μm SU-8 layer on a quartz plate as filter (see Fig. 6).

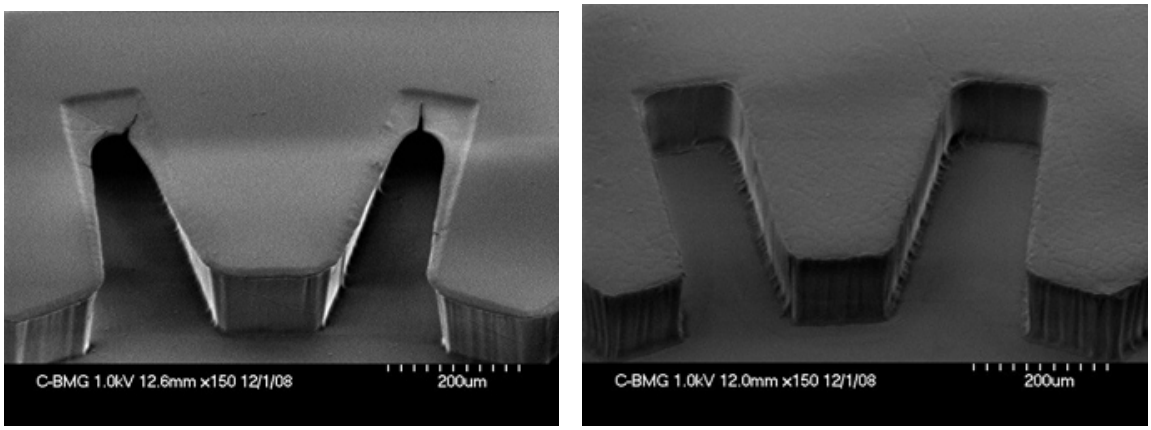


**Figure 6** The *T-topping* effect (left) and its elimination by the use of a SU-8 filter (right)

Even when quartz and SU-8 appear transparent to UV-light, the filter arrangement does attenuate the incident intensity on the SU-8 film. In order to properly expose the film is thus necessary to take the attenuation factor of the filter into account and adjust the exposure dose accordingly. Furthermore, as it will be seen below, the implementation of a back-exposure arrangement adds another attenuation factor, that of PET film, that also needs to be accounted for. Table 3 gives the transmittance and absorption percentages of

PET and the filter employed in this work (values of the filter are highly dependable on process conditions and are not recommended to be taken as reference for other works). In order to account for elements present in the optical pathway between the UV lamp and the SU-8 film (see Fig. 7) and adjust the experimental exposure dose accordingly, the following relation must be obeyed:

$$\text{Experimental dose} = \frac{\text{Recommended dose}}{t_1 * t_2 * t_3 * \ldots * t_n} \quad (1)$$

Where t denotes UV transmission percentage of an element n on the optical pathway. Recommended dose is the value recommended in SU-8 processing datasheet while experimental dose is the one to be implemented. For example, if back-exposure is to be conducted through 70 μm PET film and the filter used in this work and the recommended dose is 500 mJ/cm$^2$, the experimental dose is then 3780.92 mJ/cm$^2$. This relation allows for the adjustment of dose values (mJ/cm$^2$) in the Film thickness vs. Exposure dose recommended in the SU-8 processing datasheet. Fig. 8 shows an adaptation of this relation along with suggested optimal ranges, obtained experimentally, for exposure dose depending on the area of the pattern to be exposed. Large area patterns (> 500 μm$^2$) require more exposure dose than small area patterns.

**Table 3** Transmission and Absorption percentage for PET and filter

| Element | Transmission % | Absorption % |
|---|---|---|
| 70 μm PET (Mylar®) film | 83.13 | 16.87 |
| Filter – 50 μm SU-8 layer on quartz plate | 15.908 | 84.092 |

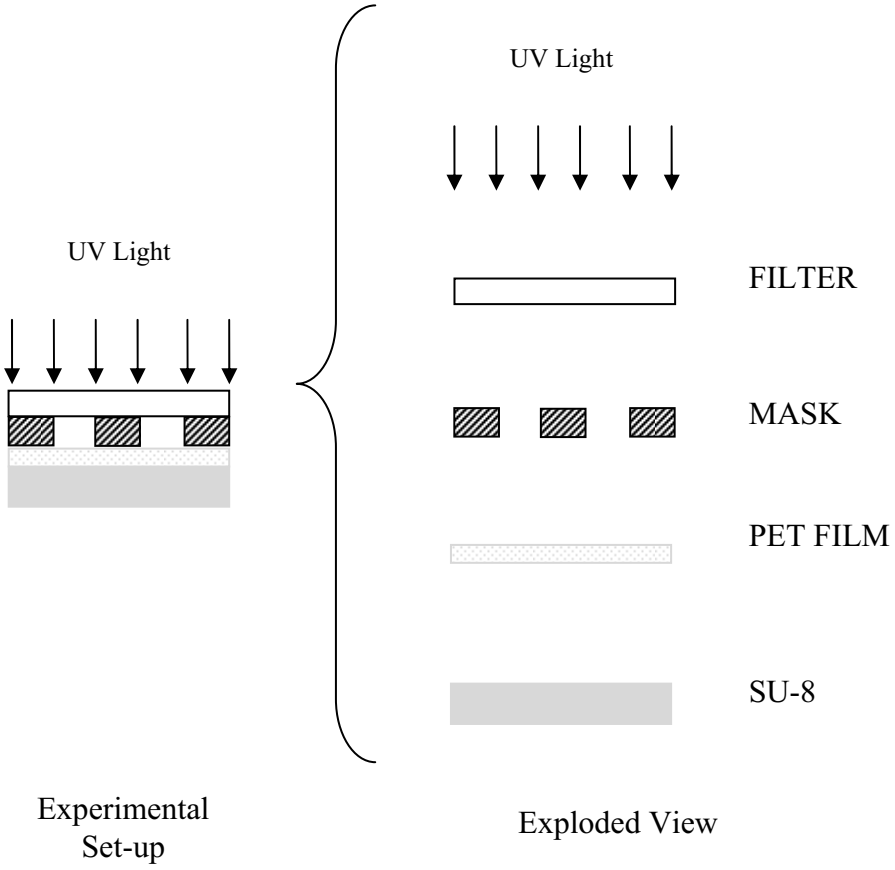


**Figure 7** Optical pathway between UV lamp and SU-8 film

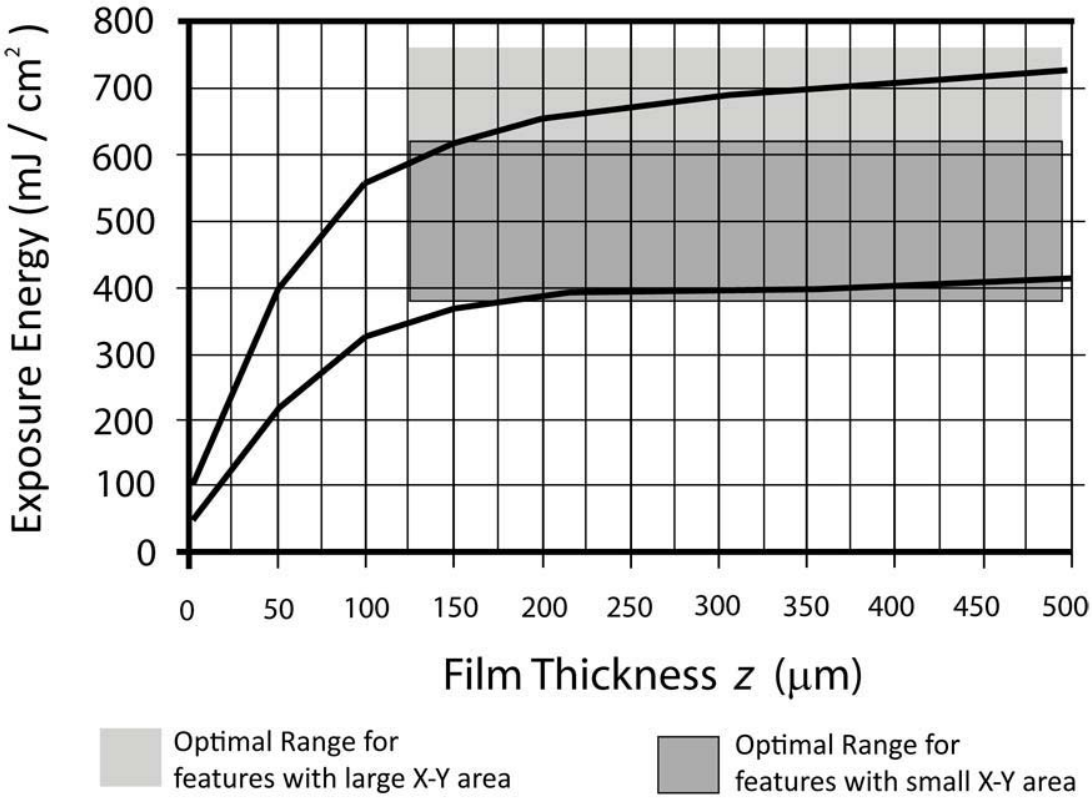


**Figure 8** Required exposure energy as film thickness varies

A key improvement to the process is the capability to conduct back-exposure on a flexible transparent substrate. This is enabled by the use of PET film as substrate. It was noted above that an ideal mold features a wall slope of 90° or slightly wider (90-95°) to facilitate demolding. The logic to follow to obtain positive slope walls on the final part depends on the type of photoresist being used. In the case of positive photoresists exposed from a top light source, diffraction effects generated at the mask-film interface cause a negative slope (<90°) on the mold wall that prevents a clean demolding step (See Fig. 9A). However, if exposure is done from the back, by shining light through a

transparent substrate, the wall slope reverses becoming positive (> 90°) (Fig. 9B). Diffraction effects occur in both cases but they are exploited to the benefit of the mold when employing back-exposure. In the case of SU-8, and negative photoresists in general, cross-linking is induced as light shines upon selected areas. The application of the same diffraction principle discussed in the case of a positive photoresist would dictate walls with positive slopes when using top-exposure and negative slopes with back-exposure. Based on experimental observation, different mechanisms, other than diffraction, are suspected to be responsible for the different cases of wall slopes in the case of negative photoresists. A theory is based on the fact that the amount of cross-linking acid generated during exposure depends on the dose delivered to the resist (recall dose = light intensity multiplied by time = exposure energy). When implementing a top-exposure arrangement (Fig. 9C), the layers on the top of the film receive more energy and thus a larger acid amount is generated when compared to the polymerizing agent created in the bottom of the film. Furthermore, as the top layers of the film become exposed, their UV transmittance diminishes [96] effectively attenuating the UV light meant to induce cross-linking in the layers underneath. Because of the energy gradient present during exposure, a concentration gradient of the cross-linking acid is also obtained. The presence of a saturated concentration of acid on the top layers induces an acid diffusion around the exposed area and broadens the pattern originally intended (a soft *T-topping* effect). The result is a negative wall slope that resembles the one obtained by taking diffraction effects into account with positive photoresists (Fig. 9A). The diffusion effect is expected to be responsible for the negative slopes commonly seen in SU-8 walls (Fig. 21A). By implementing back-exposure through a transparent substrate

(Fig. 9D), the same mechanism is reversed such that more cross-linking acid is generated on the part of the film attached to the substrate and less acid on the other side (the one to become the top of the mold). This leads to positive wall slopes on the final SU-8 mold (Fig. 21B). Even when a back-exposure procedure can be easily implemented with any transparent substrate, glass or quartz for instance, the use of transparent films, such as PET, provides a flexible substrate which enables the clean release of the SU-8 mold from the film at the end of the process; a challenging fact when using glass or quartz. Unfortunately, polyimide efficiently filters UV light and thus cannot be used for back-exposure.

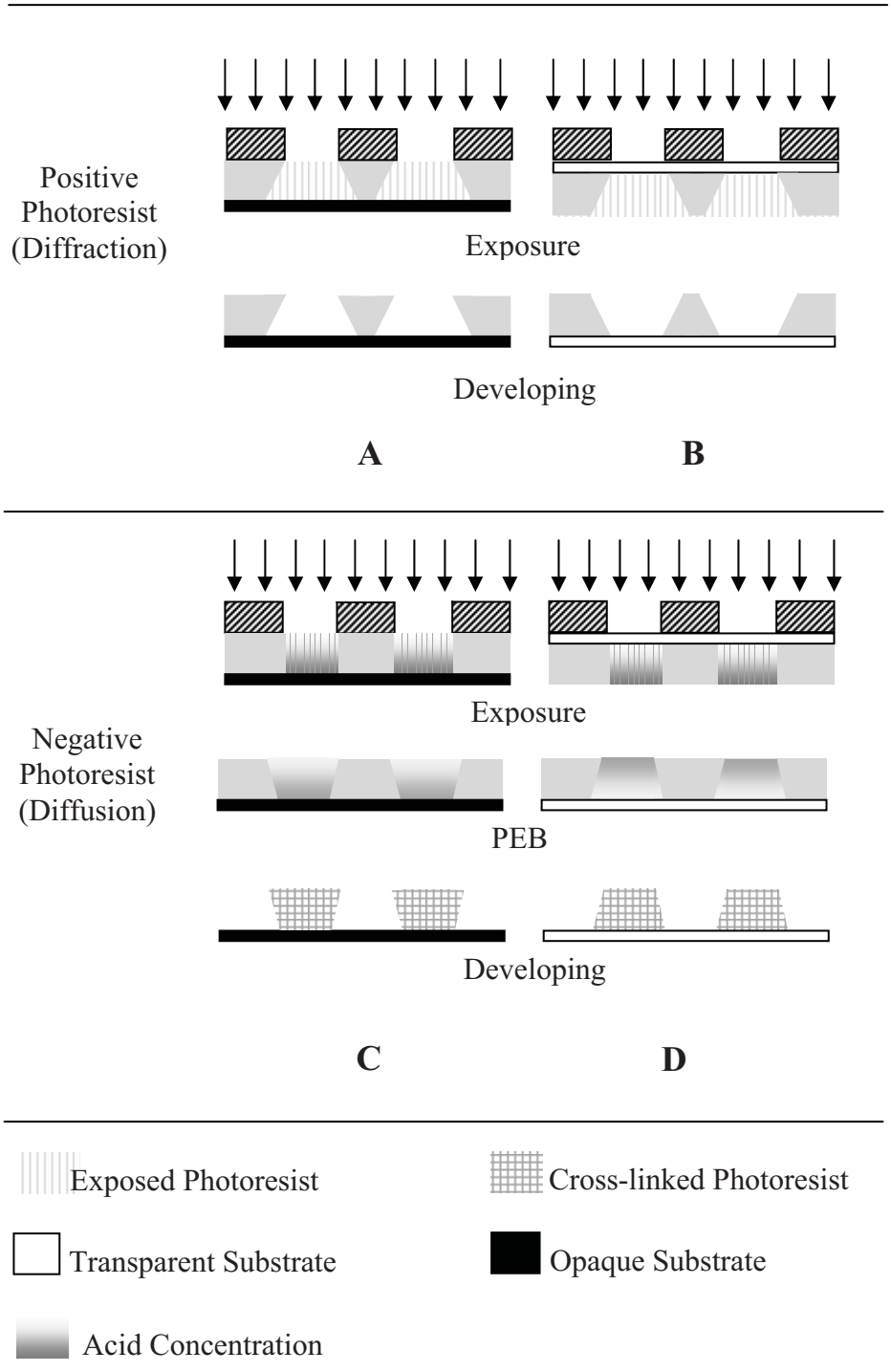


**Figure 9** Different wall slopes obtained in positive and negative photoresists a) without (negative slope) and b) with (positive slope) back-exposure

If the mold design features structures within structures, a mold for a nut or gear for example, and the goal is to obtain a free standing SU-8 part, a holding substrate must then be fabricated. Several ways were implemented to achieve this. The simplest ones were to fabricate the desired SU-8 structures directly on polyimide or polyester films. The preferred alternative is to first pattern holding substrates, say 1 $cm^2$ squares, on a thick SU-8 layer and then fabricate the desired SU-8 structures, using top or back-exposure[4], on top of the squares (Fig. 10). After the process, the PET film that held both SU-8 layers, substrate and features, is peeled off yielding free standing all-SU-8 molds featuring structures within bigger structures. It will be seen in Chapter 3 that the all-SU-8 approach is preferred over the use of polyimide or polyester as holding substrates for smaller structures within larger ones. The main reason for this is that although both PI and PET carbonize, they do not share the same CTE with SU-8 and thus thermal expansion stresses are introduced in the carbonization process (refer to Table 1). A part fabricated completely out of SU-8 does not suffer from these stresses and creates carbon molds with better fidelity to the intended design. Table 4 illustrates the advantages and disadvantages of different substrates.

[4] In the case of back-exposure, one must take into account the fact that the pre-fabricated SU-8 substrate squares are in the optical pathway and their attenuation must be considered. At the same time, the SU-8 holding substrate can also act as a filter for shorter UV wavelengths.

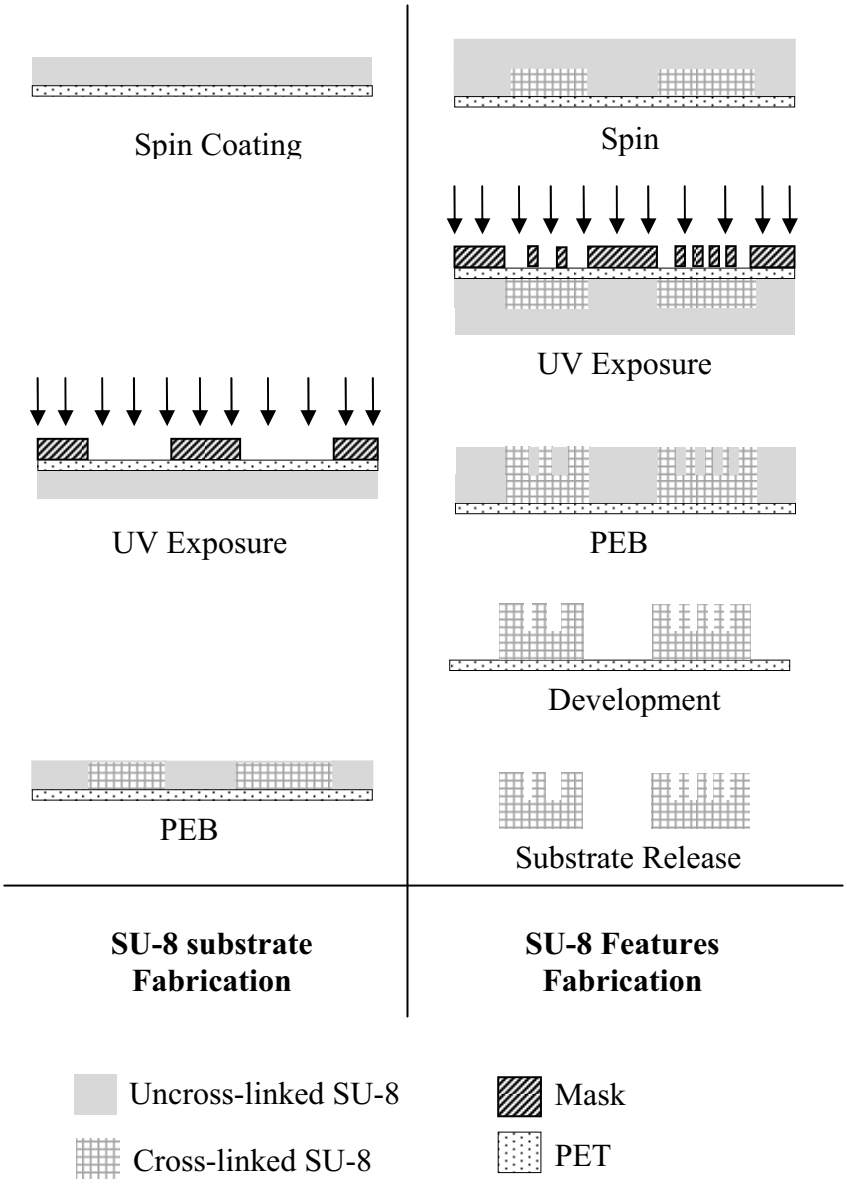


**Figure 10** The fabrication of holding substrates and SU-8 patterns with a two-layer process

**Table 4** Advantages and disadvantages of different substrates

| Substrate Properties | | TE | BE | Example | SR | C |
|---|---|---|---|---|---|---|
| Opaque | Rigid | YES | NO | Silicon | Challenging | NO |
| Opaque | Flexible | YES | NO | Polyimide | Easier | YES |
| Transparent | Rigid | YES | YES | Glass, Quartz | Challenging | NO |
| Transparent | Flexible | YES | YES | Polyester | Easiest | YES |

TE= Top-exposure, BE= Back Exposure, SR = Substrate Release, C=Carbonizes

The two-layer SU-8 process exposed above (Fig. 10) also allows for the creation of complex molds featuring undercuts and overhangs and can be expanded to n-layers. This multi-layer process requires the individual processing of n layers and the precise alignment of different masks, which might vary with layer, during exposure. Even when any substrate might be used to carry such process the use of transparent films still offers the same advantages discussed above.

Multi-layer photolithography can be a tedious and long process especially if high aspect ratio structures are being fabricated. Alternatives to multi-layer photolithography to achieve *Grayscale Lithography* were also explored in this work. The first alternative consisted on the sequential exposure of different masks on the same layer and at the same exposure step. Top or back-exposure, or a combination of both, might be employed. A very thick SU-8 layer was spin coated on a PET film and soft baked for 16 hours. After removing nuts and bolts in order to obtain a planar topography that enabled the use of the MA-6 aligner, the mask with the features of the mold was first used to back-expose the SU-8 layer with the goal of transferring the pattern along its complete thickness (dose

was 4000 mJ/cm$^2$ employing back-exposure and filter). Immediately after, the mask was changed to the one containing 1 cm$^2$ squares. In this particular case, because of the use of a negative photoresist, back-exposure is required[5]. Back-exposure through the filter was employed again but this time the dose was reduced to 200, 450, 900 or 1800 mJ/cm$^2$. The goal of this second step is to only expose a percentage of the SU-8 thickness that is enough to act as a holding substrate (Fig. 11). In this way the process time was cut in half since it only required the deposition of one layer instead of two to obtain a two level topography. Even when the mold features were correctly developed using a final dose ranging from the 4500 to 5800 mJ/cm$^2$ the intended holding substrate could not be properly fabricated[6]. This failure is believed to be attributed to either of two causes: 1) short PEB times that prevented full cross-linking or 2) to the fact that the dose was changed in function of the exposure time only (recall that dose is given by the product of incident light power density times exposure time) while the incident light power density remained the same (10 mW/cm$^2$ in this case). SU-8 is practically transparent to wavelengths above 360 nm for thicknesses up to 2 mm. By keeping the light power density constant, a cross-linking reaction is induced all along the thickness and the concentration of acid generated thus only depends on the exposure time. Less exposure time means less acid concentration generated in the film which translates to the requirement of more thermal energy during post exposure bake to complete the cross-linking reaction. This is in contrast to keeping the time constant and attenuating the

[5] Top-exposure might also be used but special care must be taken to pattern access gates for the developer to reach all un-cross-linked volumes.

[6] The first mask was exposed a total of 4000 mJ/cm$^2$ plus either 200, 450, 900 or 1800 mJ/cm$^2$ of the substrate layer. A total exposure of 5800 mJ/cm$^2$ was found to be optimal to expose the complete thickness of the 300-400 μm layer.

incident light power density. In this case, cross-linking is induced only on those parts where the attenuated light is able to reach. Acid is not generated in those parts where light couldn't reach. With the proper amount of thermal energy the cross-linking reaction finishes where acid is present and a two level topography is thus achieved.

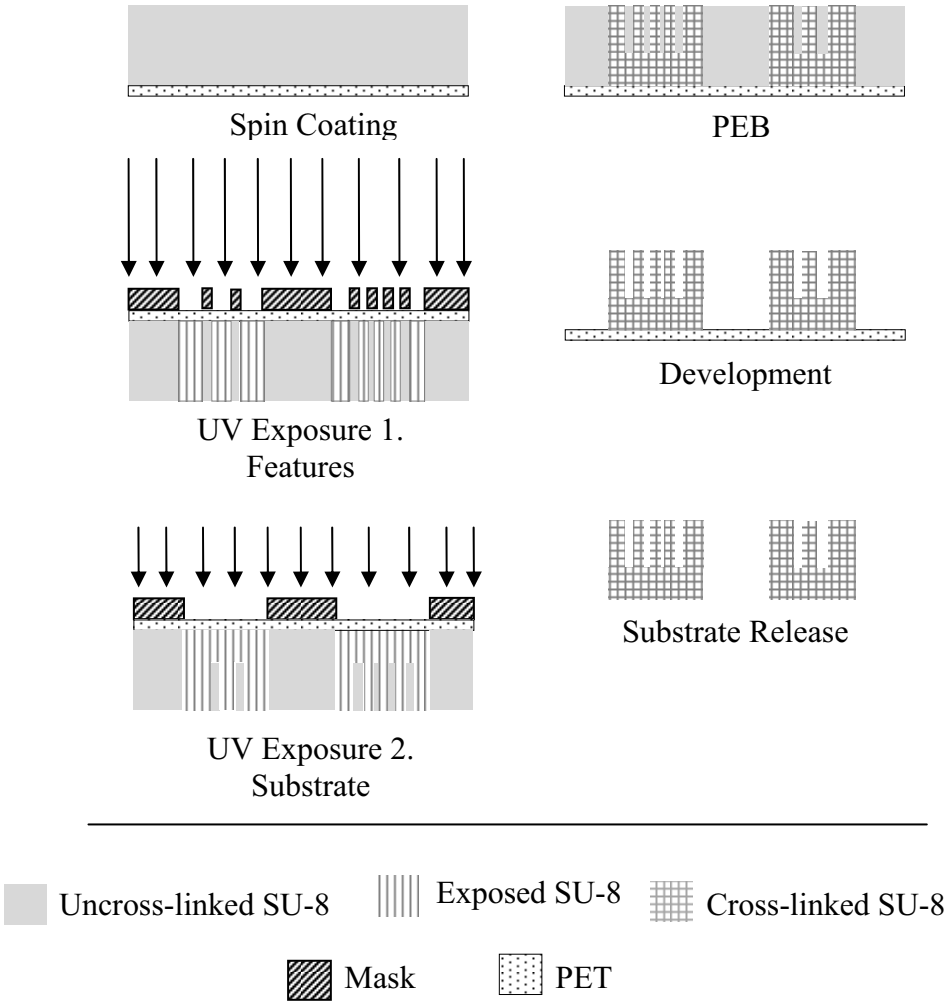


**Figure 11** Fabrication process for one-layer multi-exposure *Grayscale Lithography*

The results suggest that insufficient PEB times are the cause to blame. This theory is supported by a series of facts. Fig. 12 shows similar thickness mold features as the exposure time is increased from 116.8 to 200 and 250 s given a power density of 10 $mW/cm^2$ and a similar PEB treatment is conducted after exposure. The surface roughness is demonstrated to diminish as exposure time increases. Since cross-linking depends on the proper combination of exposure dose (light intensity * time) and PEB times, this suggests that lower exposure times are not enough to fully crosslink the polymer given a PEB time. Fig. 13 shows a series of pictures showing how the substrate layer behaves as the exposure time increases. An exposure time of 20 s did not yield any discernable substrate layer since the dose on the film was only 26.44 $mJ/cm^2$ (see equation 1) and such value is not expected to induce any cross-linking. Exposure times of 45 and 90 s (59.50 $mJ/ cm^2$ and 119 $mJ/cm^2$ respectively) yielded an increasing thickness of the substrate layer. Even when the thickness increases as expected (Fig. 13), the substrate layer is never fully cross-linked as it can be concluded from the pictures. This is believed to be a consequence of insufficient PEB times.

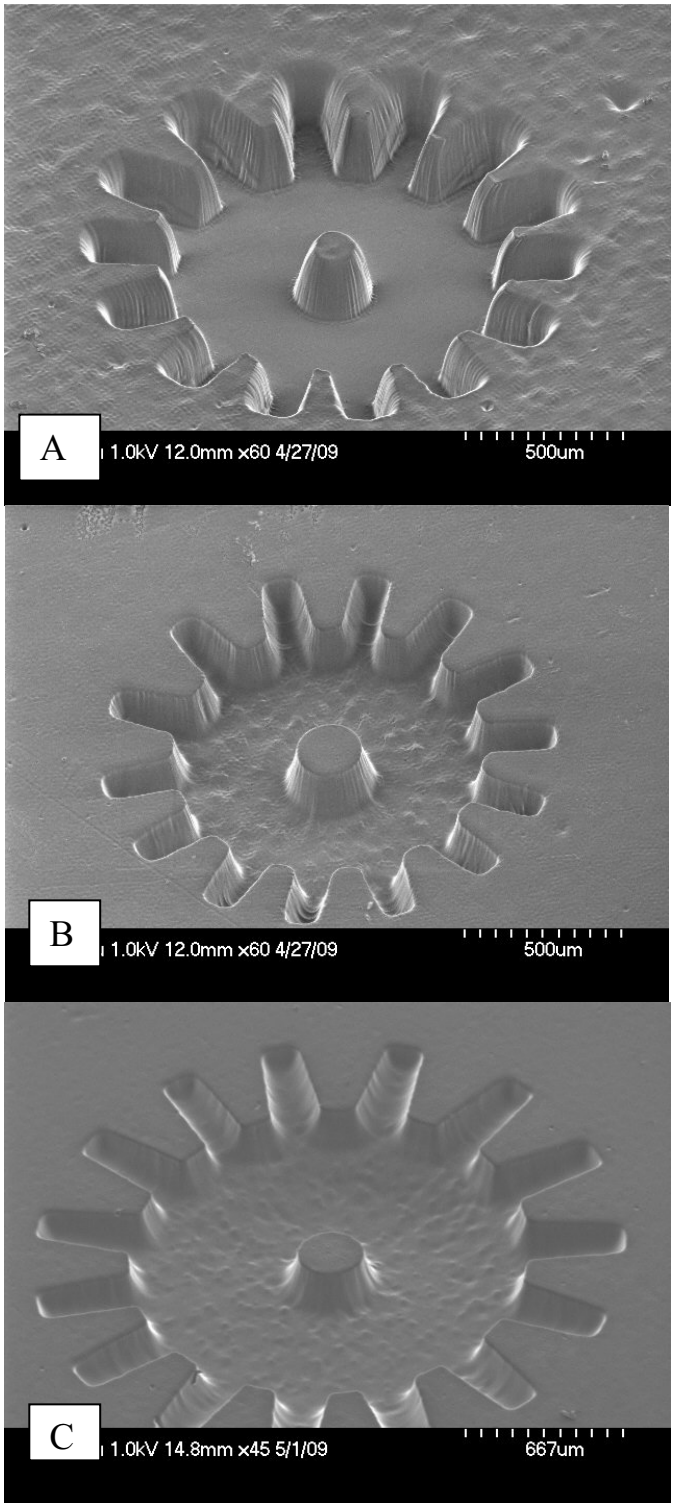


**Figure 12** Surface roughness on the top diminishes as exposure dose increases**:** A) 154**.**46, B) 264.39 and C) 330.6 mJ/cm$^2$, when keeping all other parameters constant

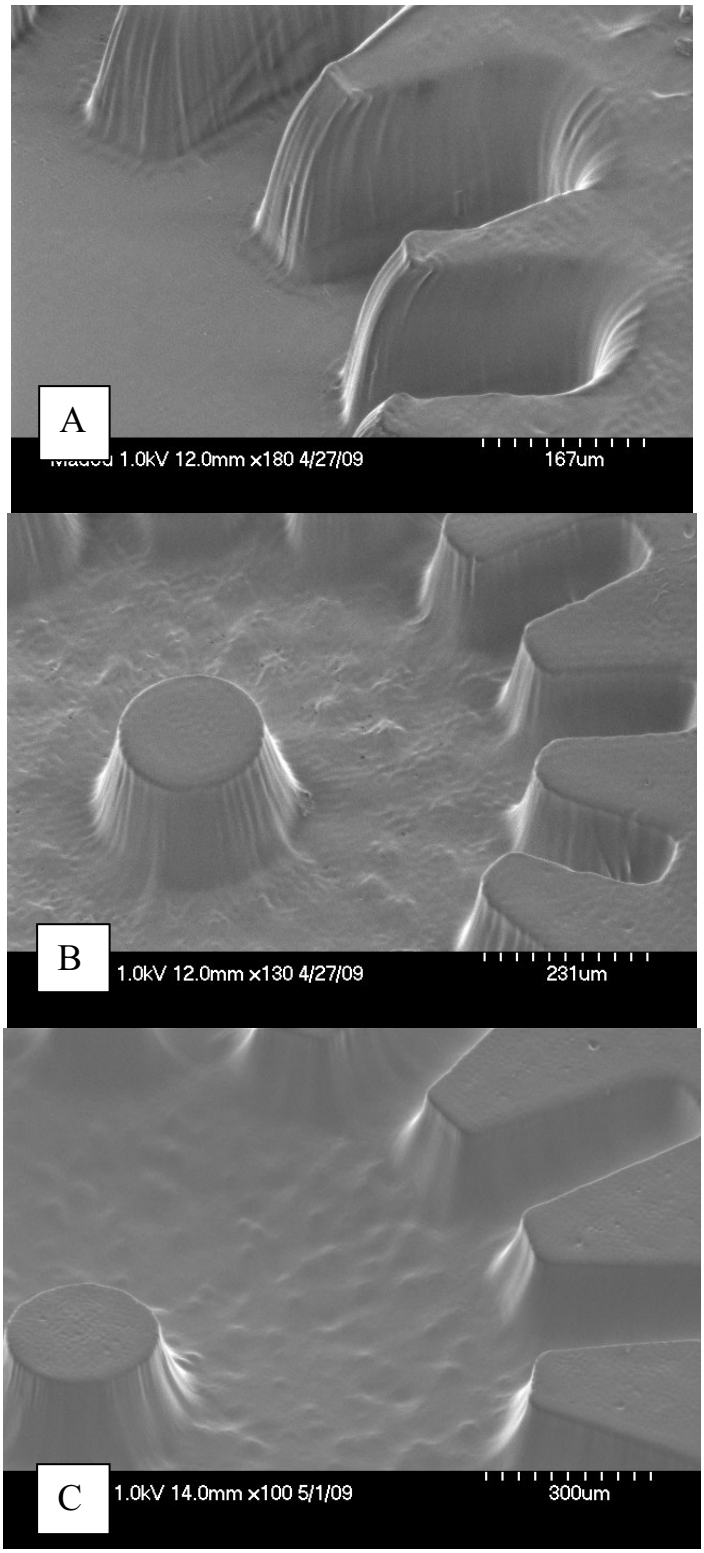


**Figure 13** Substrate layer thickens as exposure dose increases from A) 26.44 (no substrate present) to B) 59.50 and C) 119 mJ/cm$^2$

An alternative *Grayscale Lithography* technique is the variation of light intensity across the SU-8 film to obtain topographies with two or more levels. An affordable and easy way to achieve this is by employing the SF-100 Maskless Lithography System from Intelligent Micro Patterning, LLC. The SF-100 systems are based on the Digital Micromirror Device (DMD) chip from Texas Instruments Inc. (TI), and rely on the same spatial and temporal light modulation technology used in DLP (Digital Light Processing) projectors and HDTVs (high definition televisions). Different levels of light intensity are achieved by controlling the rate a mirror switches between on and off. When a mirror is switched on more frequently than off, it reflects a light gray pixel; a mirror that is switched off more frequently reflects a darker gray pixel. In this way, the mirrors in a DMD system can reflect pixels in up to 1,024 shades of gray to convert the video or graphic signal entering the DMD chip into a highly detailed grayscale image. This system was employed to derive the SU-8 structures shown in Fig. 14 using the software mask in the same figure. By correlating an RGB color value in a computer with a value of power intensity from the lamp, a process can be designed where an RGB value on the software mask yields a specific photoresist thickness. Fig. 15E shows the measured power intensity values as the RGB value changes. The RGB value shown in the X axis is the one used to set all the Red, Green and Blue values in Microsoft Paint® (for example RGB = 100 means R, G and B equal 100). RGB values of 100, 120, 140 and 160 (Fig. 15 A, B, C and D respectively) were used to expose a similar layer thickness of SU-8 with the same mask. A qualitative conclusion was reached based on the optical and SEM picture sequence 15 A, B, C, D showing how lower RGB values yield thinner SU-8 layers.

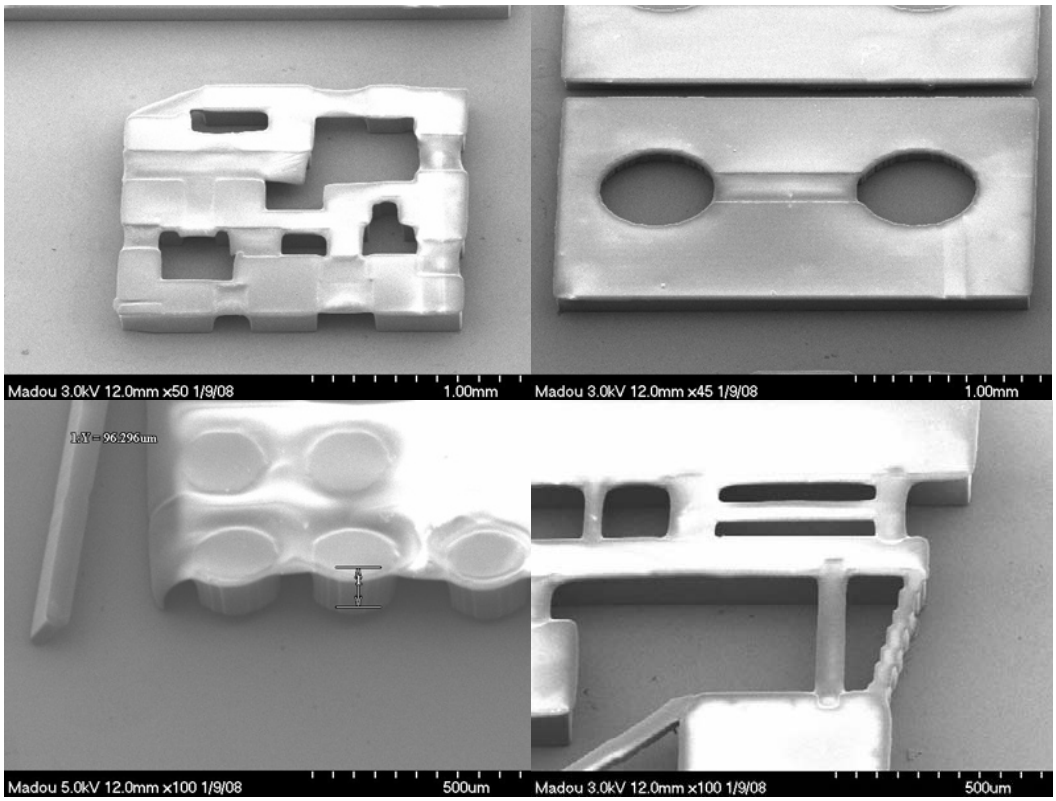


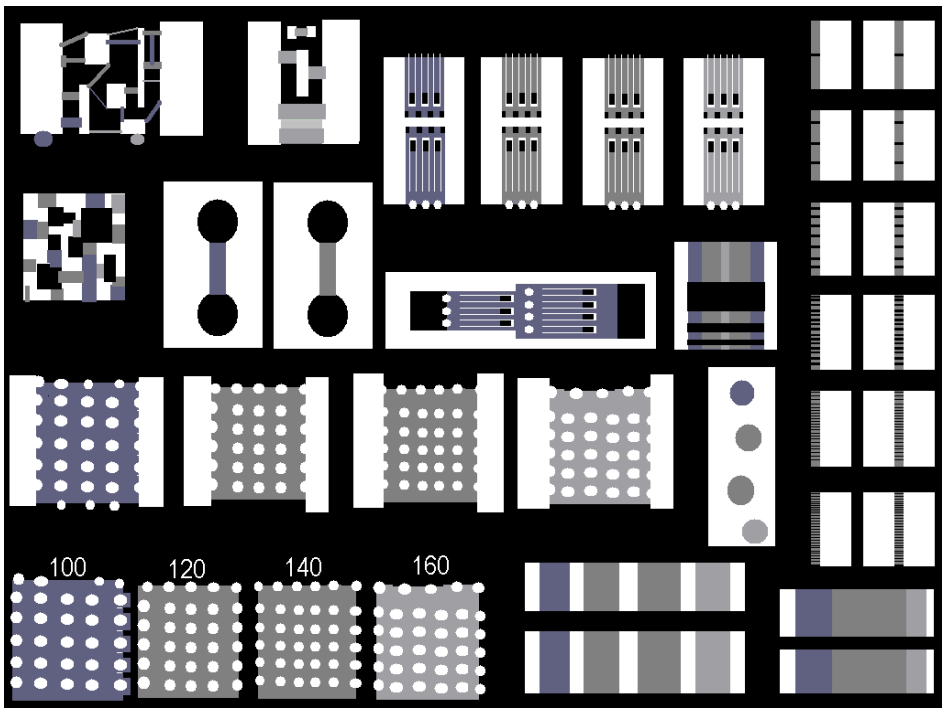


**Figure 14** Examples of *Grayscale Lithography* on SU-8 obtained with the SF-100 system and the mask used to fabricate them (bottom)

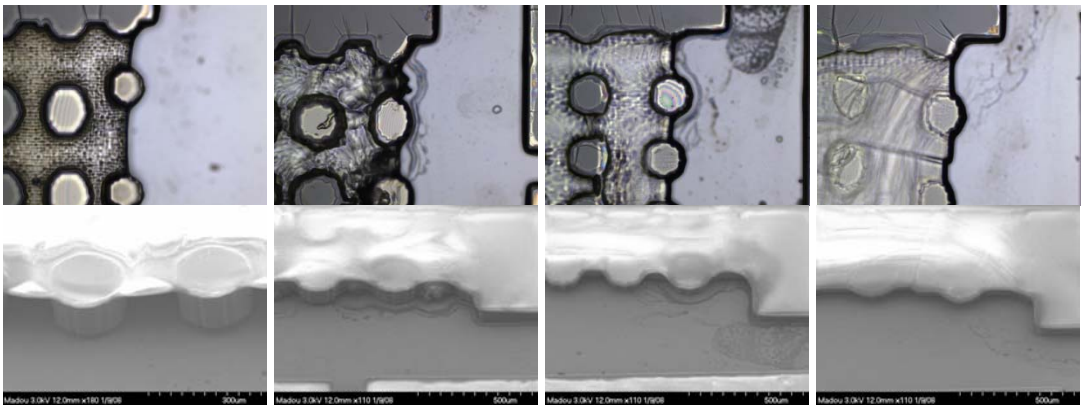

A B C D

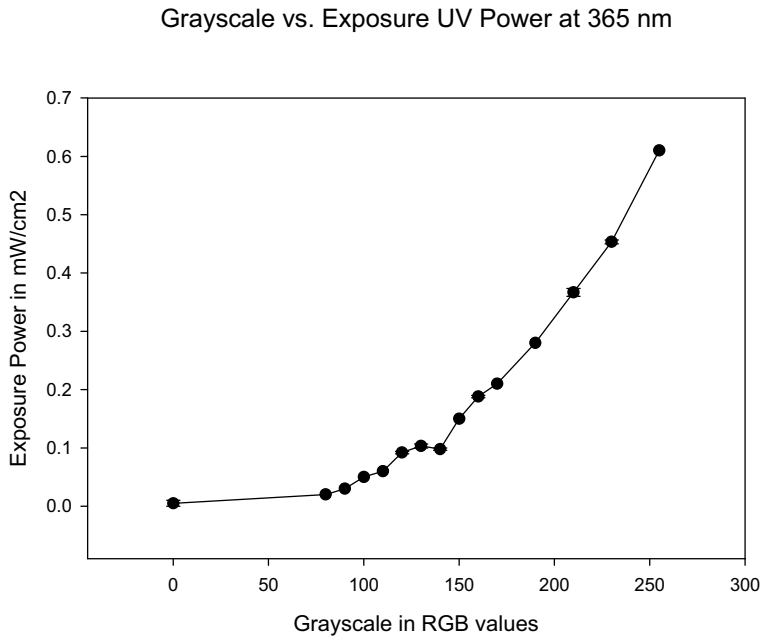


E

**Figure 15** Correlation between RGB values and resultant SU-8 thickness

*Post Exposure Bake*

A post-exposure bake (PEB) of the exposed SU-8 is required to complete the cross-linking reaction. In the case of a chemically amplified resist, such as SU-8, the post exposure bake is most critical. Although the cross-linking reaction induced during exposure continues at room temperature, it is greatly catalyzed by baking at 60-100°C. The precise control of PEB times and temperatures critically determines the subsequent development and the quality of the final features. Extended PEB times will introduce significant amounts of stress in the polymer that will most likely cause cracking on the surface, structure bending or peeling from the substrate in the worst cases; especially in extended, large surface area features. Reduced times will yield structures that are not completely cross-linked and can be attacked by the developer. This causes extremely high surface roughness or even complete dissolution. An optimal PEB improves adhesion, reduces scumming (resist left behind after development), increases contrast and resist profile (higher edge-wall angle) and reduces the effects of standing waves in a regular resist.

In order to minimize internal stresses in the structure, a similar three step PEB was conducted for all films thicker than 100 μm which yielded positive results. The baking started with a 10 minute heating at 65 °C followed by a 15-20 minute interval at 95 °C. The final step consisted of an extra 10 minutes at 65 °C. All steps were conducted in a convection oven. It is believed that PEB benefits from convection heating as thermal energy is applied all over the surface area of the polymer structure. Rapid heating and cooling of the exposed pattern should be avoided as rapid changes induce a significant

amount of stress. Thanks to the aluminum ring still attached to the polymer substrates after PEB, the exposed SU-8 film remains planar during the complete process. The fact that the coefficients of thermal expansion of PET, PI and Al are similar and approach that of SU-8 greatly reduces stresses on the interfaces when compared to the use of Si as substrate.

### *Development and Hard Bake*

Development is the dissolution of un-polymerized resist that transforms the latent resist image, formed during exposure, into a relief image that will serve as a precursor for carbonization in this case. During the development of SU-8, those areas that were not cross-linked will dissolve upon immersion in the proper developer (in this case, commercial SU-8 developer from MicroChem). Constant agitation during development is recommended to constantly feed fresh developer to the substrate and decrease developing times. However, care must be taken when developing high aspect ratio structures as excessive agitation might cause mechanical failure.

Normal development times employed in this work ranged from 5 to 15 minutes with constant moderate agitation. Developed parts were then quickly rinsed with acetone and iso-propyl alcohol, in that order, and blown dried with a nitrogen gun. Depending on the substrate used in the process, three types of SU-8 molds were obtained, SU-8 on silicon, SU-8 on polyimide or free standing SU-8. Traditional photolithography was conducted to obtain the SU-8 on silicon molds while SU-8 on polyimide molds only incorporated a few of the improvements listed in this chapter, namely the use of the film holder. The

case of free standing SU-8 molds (Fig. 16) is of most interest and is achieved by using PET film as substrate. A further advantage of the use of PET is the capability to conduct back-exposure on SU-8 to optimize the wall slope for molding applications. Thanks to the low adhesion of SU-8 to PET and to the fact that a 70 μm PET film is highly flexible, the SU-8 parts could be easily peeled off complete from the PET film by just bending the film. Parts could be peeled off from PI films in a similar way but retrieving complete parts proved to be a challenge given the higher adhesion of SU-8 to PI.

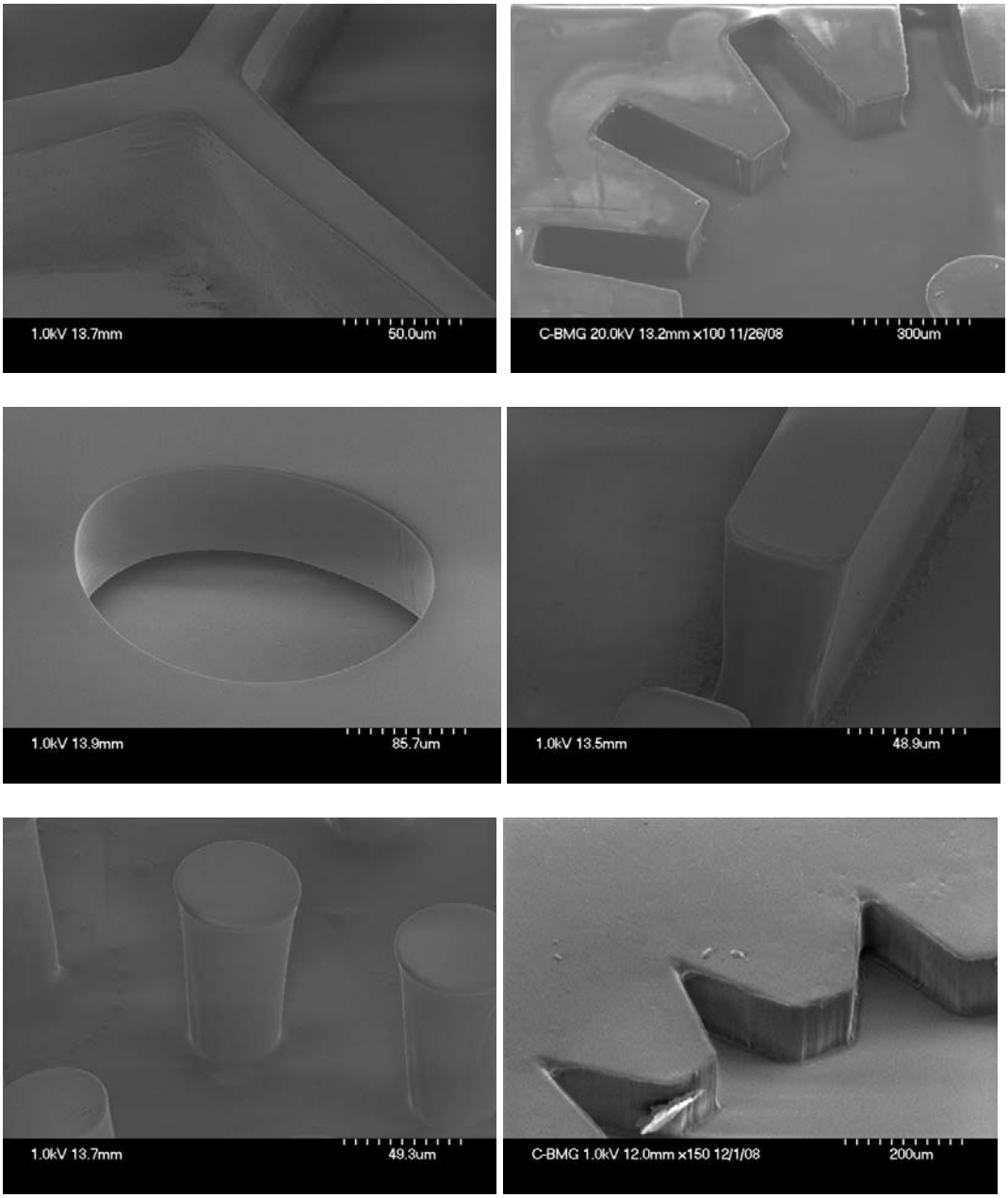


**Figure 16** Free standing SU-8 micro molds

# CHAPTER 3. Fabrication Process II: Carbon Micro Molds and BMG Forming

This chapter deals with the derivation of carbon molds from the SU-8 precursors fabricated in Chapter 2, the process of BMG thermoplastic forming and the demolding of the BMG parts.

## *Carbonization*

Carbonization is the process by which solid residues with a high content of carbon are obtained from organic materials, usually by pyrolysis in an inert atmosphere [103]. Different precursors to obtain glass-like carbon, other than photoresists, may be used and include phenolic resins, polyfurfuryl alcohols, cellulose, polyvinyl chloride and polyimides [29, 41, 42, 56, 61, 104-112]. The mentioned precursors do not melt during the carbonization process but rather maintain their shape along the process thus allowing the derivation of patterned or shaped carbon pieces. However, different degrees of shrinkage and carbon yield (the ratio of the weight of carbon to the weight of the original polymer sample) are obtained during carbonization depending on the precursor used. In the case of photoresists, volume shrinkage varies from 50 to 90% [62, 66, 67, 70]. As with all pyrolytic reactions, carbonization is a complex process with many reactions taking place concurrently, including dehydrogenation, condensation, hydrogen transfer and isomerization [113-121]. The pyrolysis process of photoresists, and organic

compounds in general, can be divided into three major steps: pre-carbonization, carbonization and annealing. Important is to recall now that SU-8, being a thermoset resin, has an amorphous structure consisting of aromatic molecules that are randomly dispersed. The first step of pyrolysis is pre-carbonization. During pre-carbonization ($T < 573$ K) molecules of solvent and unreacted monomer are eliminated from the SU-8 matrix. The carbonization step can be further divided into two stages. From 573 to 773 K (300 to 500 °C), heteroatoms such as oxygen and halogens are eliminated causing a rapid loss of weight, but a minimal volume shrinkage, while a network of conjugated carbon systems is formed (*i.e.* carbon ribbons are formed). Hydrogen atoms start being eliminated towards the end of this stage. The second stage of carbonization, from 773 to 1473 K (500 to 1200 °C), completely eliminates hydrogen causing the carbon ribbons to move together. This carbon network crumbling causes a significant loss of volume but a minimal change in weight. At this point, permeability decreases and density, hardness, Young's modulus and electrical conductivity increase. The final step, annealing, is carried out at temperatures above 1473 K, to allow the gradual elimination of any structural defects and evolve further impurities [41]. The final pyrolysis temperature determines the degree of carbonization and the residual content of foreign elements. For instance, at $T \sim 1200$ K the carbon content of the residue exceeds a mass fraction of 90% in weight , whereas at $T \sim 1600$ K more than 99% carbon is found [29, 118, 122].

For this work, pyrolysis was conducted on a Thermco Mini-Brute MB-71 diffusion furnace featuring a quartz tube. Nitrogen gas was flowed at 2000 sccm during the process to create an inert atmosphere in the tube. All pyrolysis processes featured a final

temperature of 900 °C. The heating ramp was conducted in two steps with a 30 minute interval in between them. First ramp was from 0 to 300 °C at 25 °C/min while second ramp was from 300 to 900 °C at 12 °C/min. Furnace was then held at 900 °C for 1 hour. Cooling ramp was set to 2 °C/min. The two step heating ramp, and the interval in between, is mainly conducted to completely eliminate oxygen residues, often present in negative photoresists, before high temperatures are reached and where the presence of oxygen derives in the burning of the photoresist instead of its thermal degradation to glass-like carbon[67].

The pyrolysis process yielded different results depending on the substrate employed. Recall that after the photolithography process three different mold designs were obtained: SU-8 on silicon, SU-8 on polyimide and free standing SU-8 (SU-8 pattern on a SU-8 substrate). While polyimide and SU-8 carbonize, silicon does not thus two types of final carbon molds are possible: carbon-on-silicon or all-carbon. At this point is important to note that the pyrolysis of high-surface-area SU-8 patterns on a rigid substrate has so far only been successfully demonstrated with silicon wafers, or wafers coated with silicon oxide. Quartz has been previously tried but the large mismatch between the coefficients of thermal expansion (CTE) of quartz ($0.59\ 10^{-6}$/K) and the resultant glass-like carbon after pyrolysis ($2.2\text{-}3.2\ 10^{-6}$/K) has caused the patterned carbon to curl and peel from the quartz substrate. Few other practical materials are able to withstand the required temperatures for pyrolysis making the choice for substrate quite limited. The use of silicon as substrate offers a CTE of $2.6 – 4.3\ 10^{-6}$/K and allows the obtainment of glass-like carbon patterns on a flat substrate. However, experimental results have shown

that the successful derivation of a carbon pattern on a silicon-based substrate depends on the SU-8 precursor dimensions. Specifically, the X-Y surface area that must be patterned in the polymer to obtain a carbon structure reduces as the thickness, or Z dimension, increases. For example, SU-8 films thicker than 20 μm must be patterned in features with a surface area less than 200-300 $\mu m^2$. A 4" wafer can be easily coated with a 1-2 μm carbon layer if departing from a 10 μm layer of SU-8. Finally a 200 μm post with a diameter of 50 μm can be derived from a 400 μm high, 100 μm diameter SU-8 post. These parameters are given as a general guideline; a full characterization is pending to be conducted. Therefore, is a challenge to fabricate thick carbon structures featuring a large surface area on silicon-based substrates. Three different mold designs were obtained using silicon as substrate. Results are shown in Chapter 4.

The pyrolysis of SU-8 on polyimide yielded interesting results. Kapton® film or Cirlex® were used as polyimide substrates. After SU-8 features were developed and prior to pyrolysis, 1.2 $cm^2$ squares, containing the SU-8 pattern of 1 $cm^2$, were cut out with scissors. During the initial stage of pyrolysis the difference of CTE between SU-8 (50-52 $10^{-6}$/K) and polyimide (20-40 $10^{-6}$/K), together with the fact that Kapton® is flexible caused the bend up of the Kapton®-SU-8 arrangement. The resultant carbon molds are shown in Fig. 17. Important is to note that the pyrolysis of only Kapton® films of similar dimensions yielded flat carbon layers. The use of Cirlex® gave carbon molds with a lower degree of bending. However, Cirlex® substrates are not suited for carbonization. Cirlex® is basically an adhesiveless stack of polyimide films that behaves well at lower temperatures. It is believed that during pyrolysis the different layers of polyimide do not

carbonize in a uniform manner and introduce mechanical imperfections, such as bubbles, in the stack. After pyrolysis, several bubbles are present even when the resultant carbon mold is flat (Fig. 18).

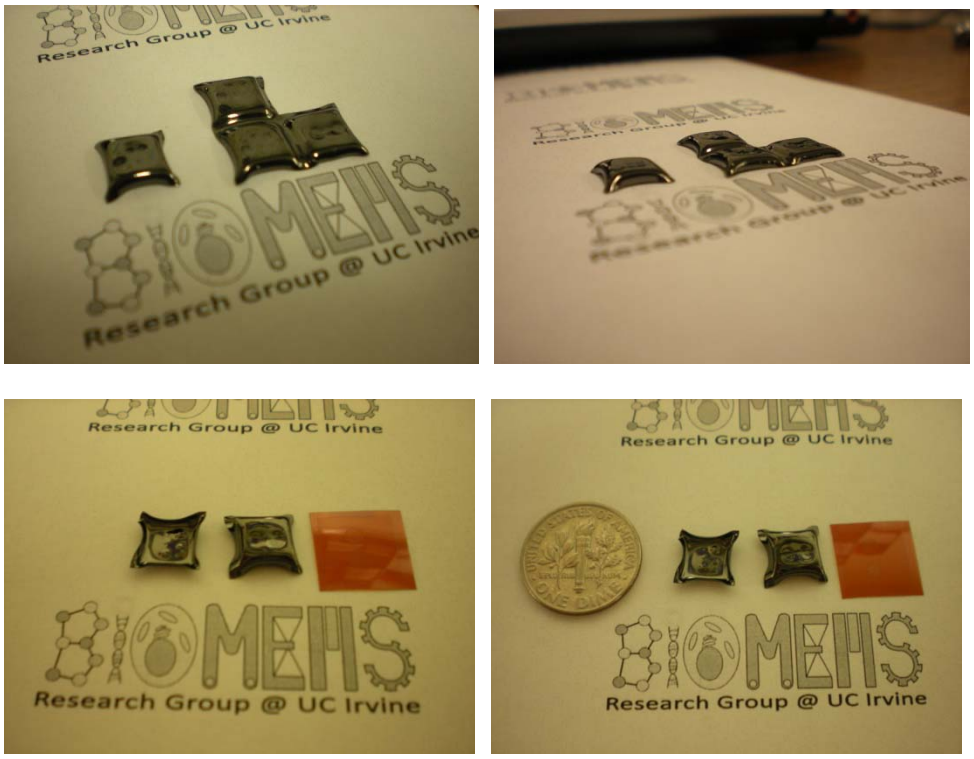


**Figure 17** Curved carbon molds derived from SU-8 patterns on a Kapton® film substrate

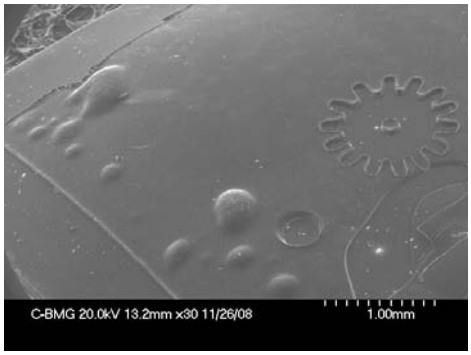


**Figure 18** Carbon molds derived from patterned SU-8 on a Cirlex® substrate

At last, the pyrolysis of free standing SU-8 molds was conducted. As a reminder, these molds were obtained by peeling out the SU-8 parts from the PET film that served as substrate during the photolithography process. In this case there are no material interfaces in the polymer part. This offers a homogeneous mold that expands uniformly as temperature varies and yielded the best results in terms of fidelity to the original design. The comparison on the use of different substrates, or no substrate, is given in Chapter 4 in the results section. To summarize, two different kinds of mold were obtained after carbonization: 1) carbon on silicon and 2) all carbon. All carbon molds were further classified as those from SU-8 on polyimide or all SU-8.

### *BMG Thermoplastic Forming*

BMG molding was not conducted by the author of this thesis but by his collaborators at Yale University, Dr. Golden Kumar and Dr. Jan Schroers. Briefly, BMG forming was conducted using custom heating plates (top and bottom) installed on a load cell of an *Instron* mechanical testing machine to allow a precise control of temperature and applied pressure during experiments. Carbon molds were heated to 430 °C by the bottom heating plate while a piece of Zr-BMG, an alloy of $Zr_{44}Ti_{11}Cu_{10}Ni_{10}Be_{25}$ also known as Vit1b, was placed on the heated mold. After allowing 30 s to equilibrate the temperature of mold and Vit1b, the applied load was increased to attain a preset pressure value of 10 MPa. The applied pressure was kept constant for varying time intervals depending on the mold type and features. For further references on BMG molding the reader is directed to [20, 22, 23, 123-125].

*Carbon mold release and sacrificial molds*

Different approaches were considered for the demolding of the BMG parts. Sacrificial molds were initially considered given the relative easiness to fabricate them and the low cost of the mold itself. Wet immersion in a variety of chemicals was first explored with unsuccessful results. Table 5 summarizes such results. A 1.56 μm carbon layer was fabricated on a 4" silicon wafer which was then diced into 1 $cm^2$ squares. One square was then immersed in 10 ml of the chosen chemical. Although no chemical used was capable of etching carbon, most of the chemicals caused the carbon layer to peel out from the silicon substrate. Acetone was found to be the one that peeled the carbon in the most rapid and uniform way. Uniform peeling refers to the fact that the layer peels off as a whole, non uniform denotes peeling in pieces.

**Table 5** Results of attempted carbon etching with different wet chemicals

| | **Etching** | **Peeling, Velocity, Uniformity** |
|---|---|---|
| $HNO_3$ | NO | Yes, Fast, Non uniform |
| $H_2SO_4$ | NO | No |
| $H_3PO_4$ | NO | No |
| HCl | NO | Yes, Moderate, Uniform |
| RCA solution | NO | Yes, Fast, Non Uniform |
| NaOH (30%) | NO | Yes, Moderate, Uniform |
| Acetic Acid | NO | Yes, Moderate, Non Uniform |
| Acetone | NO | Yes, Faster, Uniform |

Experimental results coincide with the literature in that no chemical is known to attack glass-like carbon [36, 38, 105]. Oxygen is the only element known to attack this material and only does so under certain conditions, namely high temperature or plasma environments. Thermal heating at 900 °C for an hour is routinely used by this author to

clean silicon wafers from carbon residues. However, at such temperatures few materials survive and BMGs are not one of them. Therefore, oxygen plasma is the best option to etch carbon.

The bulk removal of carbon residues from formed BMG parts was implemented with a Minilock-Phantom III Inductive Conductive Plasma/Reactive Ion Etching, ICP/RIE (TRION Technology). Oxygen plasma was generated at 7 mT of oxygen pressure and 275 W of power. Resultant etch rate was 1.2 μm/min. The use of an inductive conductive plasma (ICP) allowed for faster etch rates than those reported by some [126]. After a 10 min plasma treatment, the carbon mold is broken down and a simple sonicated bath in acetone is enough to remove most of the carbon residues. Full cleaning of the BMG part could not be achieved as pictured in Fig. 19. Residues shown are believed to be mechanically interlocked on the rough surface. On the bright side, the dashed ellipses on Fig. 20 demonstrate the capability of BMG to replicate even the finest details such as the wall roughness of the carbon mold (shown on the left of the figure).

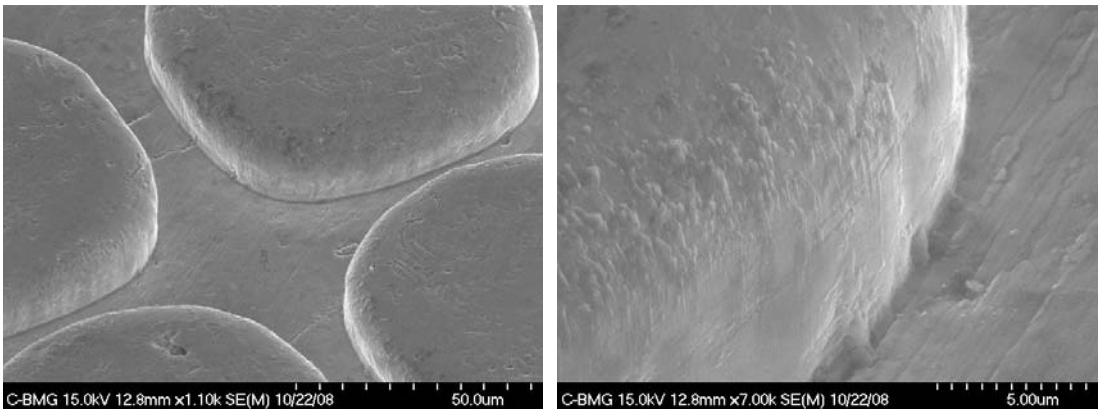


**Figure 19** Carbon residues on the BMG wall

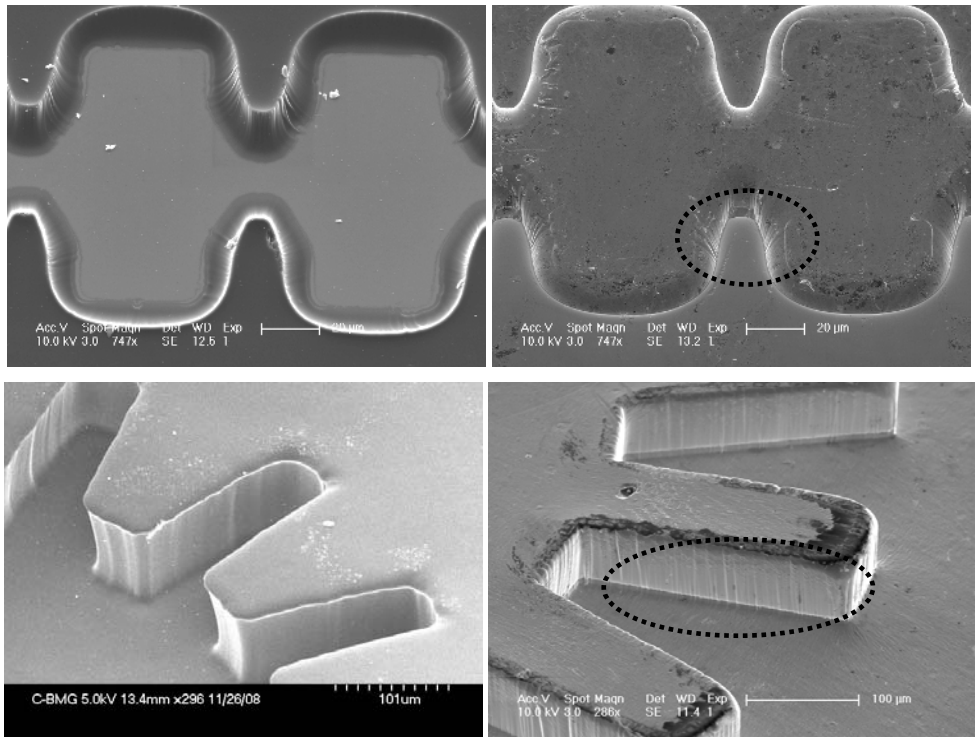


**Figure 20** Fine features replication on BMG parts (right). Carbon molds shown on left

Important is to note that BMG molding, and the subsequent oxygen plasma etching, has only been conducted with carbon molds featuring negative slopes (< 90 °C). Even when positive slopes have been achieved, these later molds have not been used for BMG forming. The use of a mold featuring walls with positive slope (see Fig. 21 right) facilitates the clean release of the part from the mold [2]. This is in contrast to the use of walls with negative slopes, as is the case of the results just shown (Fig. 21 left), that have been proven to mechanically lock the formed part in the mold. BMG forming is planned to be conducted using the new improved molds. The use of these molds featuring positive slopes on its walls together with the inertness of glass-like carbon and its resistance to be wetted by most materials are expected to enable the clean release of the BMG part.

Nevertheless, the expertise obtained on carbon etching by oxygen plasma will allow for the implementation of sacrificial carbon molds featuring overhangs and undercuts (refer to *Grayscale Lithography* results presented in Chapter 2). In this case an etching system that attacks the carbon from all directions would be preferred over a line-of-sight approach such as Reactive Ion Etching (RIE). Candidates for implementing an isotropic etch include oxygen plasma and xenon difluoride systems.

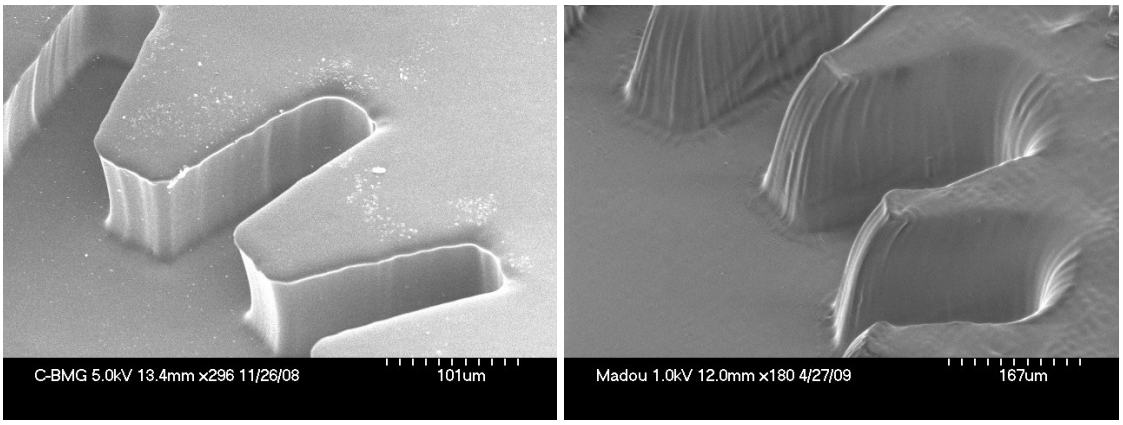


**Figure 21** Negative (left) and Positive (right) slopes on fabricated molds

# CHAPTER 4. Results and Further work

Different results were obtained depending on the kind of mold used. The first set of results was derived using carbon-on-silicon molds. The fabrication sequence for two different BMG geometries is shown in Fig. 22. SU-8 molds (Fig. 22A, B) were fabricated on a $Si/SiO_2$ substrate following a traditional UV photolithography process. Carbon molds shown in Fig. 4.1C and D were obtained by pyrolysis of these SU-8 molds and were then used to TPF the BMG following the method detailed above. Carbon molds were then released by mechanical means (Fig. 4.1E, F). Oxygen plasma was relied on to remove the bulk of the remaining carbon (Fig. 4.1G and H) from the BMG while an acetone bath with sonication was used to remove carbon residues. Finished BMG parts are shown in Fig. 4.1I and J. Other BMG structures fabricated with the same process are shown in Fig. 23. A minimal gap of 2 μm was obtained by this process (Fig. 24).

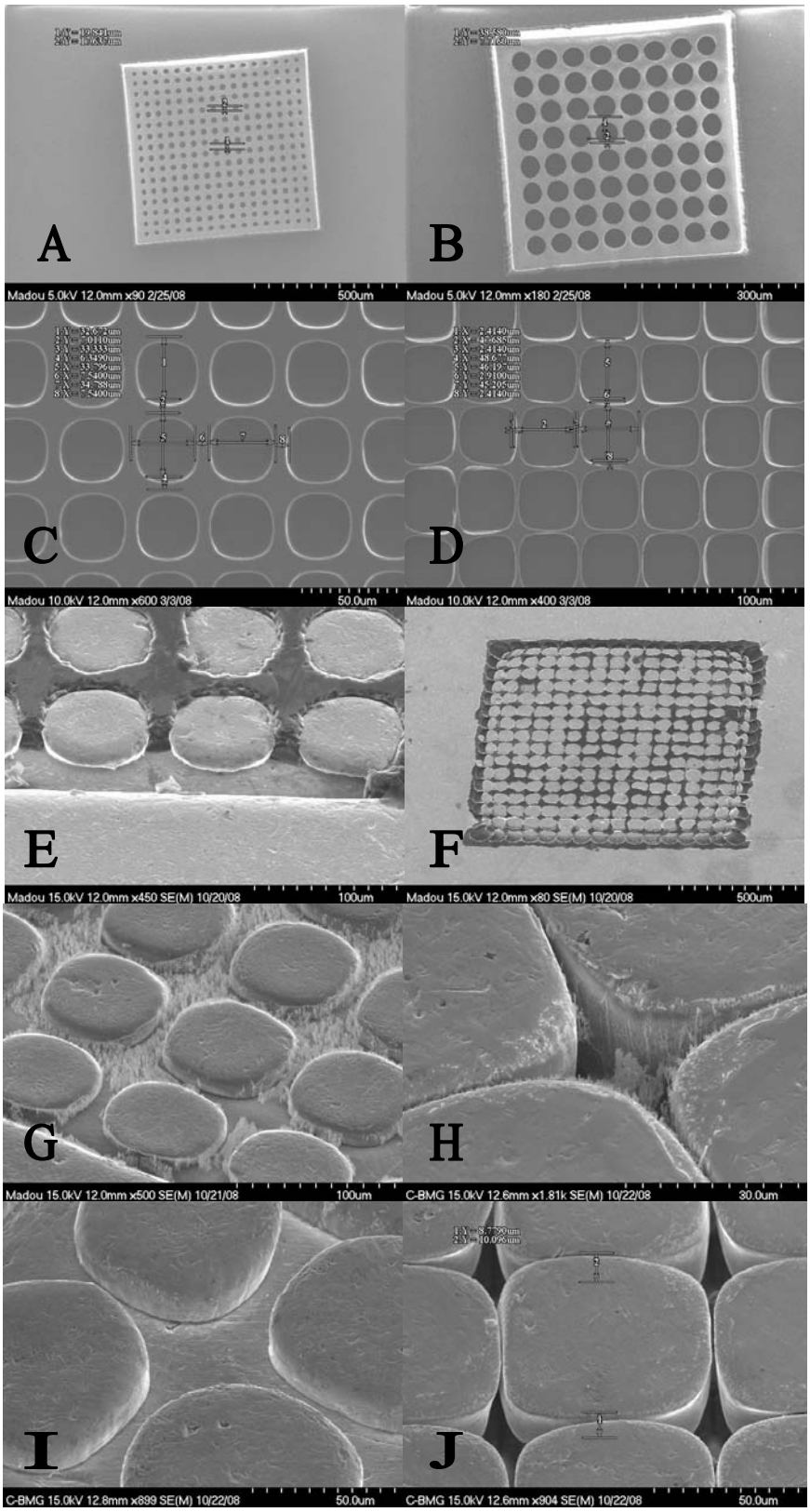


**Figure 22** Fabrication sequence for carbon-on silicon molds

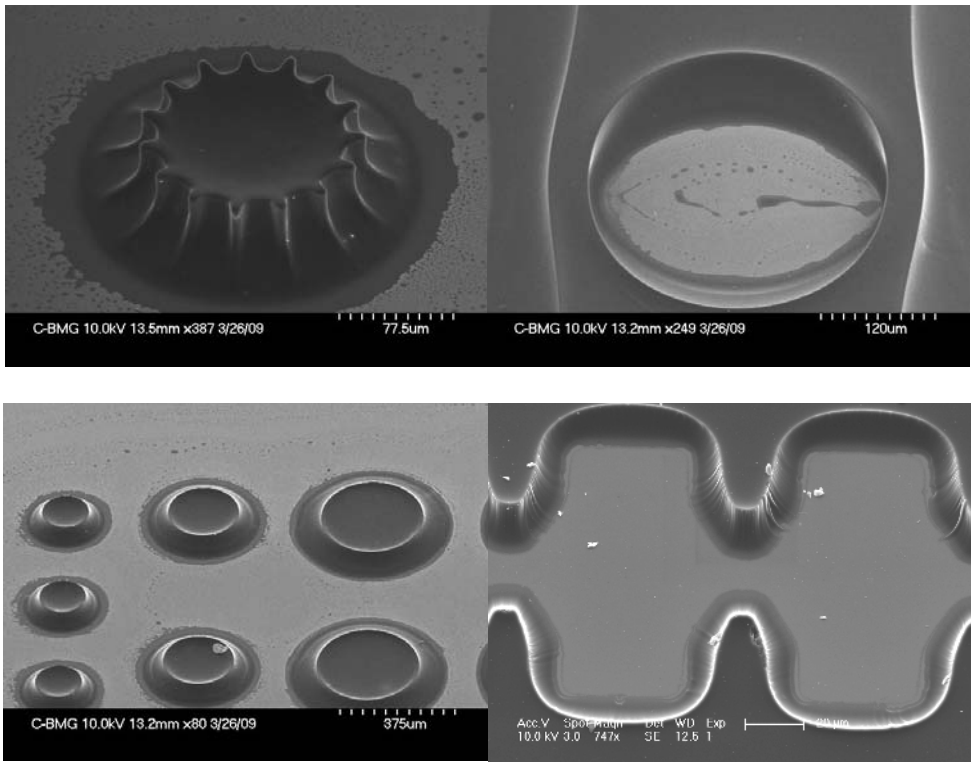


**Figure 23** Other carbon-on-silicon geometries

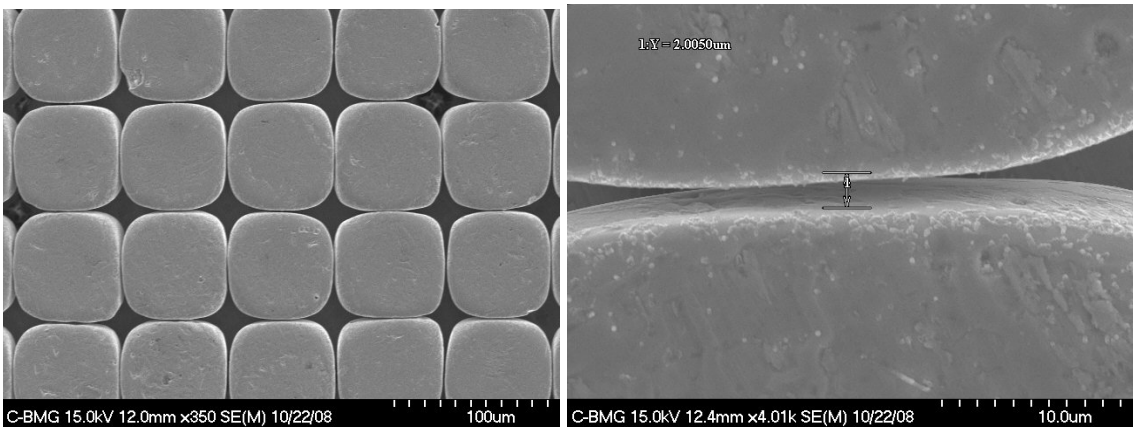


**Figure 24** Achieved 2 μm gaps between BMG structures

The first important refinement to the fabrication process presented above was the elimination of the silicon substrate. The incorporation of alternative substrates such as polyimide and polyester films allowed the fabrication of free standing carbon molds. It was already mentioned that the use of polyimide as substrate derives in curved carbon molds (Fig. 17) given the difference in the coefficients of thermal expansion (CTE) between SU-8 and polyimide. Even when free standing carbon molds could be derived in that manner, the fabrication process did not yield an acceptable geometry and had poor reproducibility. It was obvious then that stresses due to mismatches on the thermal properties of the precursor materials had to be eliminated. The second improvement was the incorporation of a releasable substrate in the process. Based on the printed-circuit-board (PCB) industry experience, a PET film was selected to be used as peel-off substrate[7]. As mentioned before, the use of PET film allowed for its easy and clean release from the SU-8 mold before pyrolysis. Important is to note however, that PET film should be released after the developing step and not prior. Attempts to remove it prior to development resulted in mechanical deformation of the mold as the adhesion of uncross-linked SU-8 is significantly higher than that of its cross-linked version. The use of a releasable PET film, besides reducing processing costs, eliminates stresses at the interface of different materials since the mold to be pyrolyzed is composed only of SU-8. Recall that in Chapter 2, in the Exposure section, two different processes for SU-8 patterning when using PET substrates were detailed. One of them consisted on the direct fabrication of SU-8 molds on PET and the other was the fabrication of SU-8

[7] PCBs are usually patterned using a photoresist mask. This mask is obtained by the lamination of a dry thick photoresist on the board and its subsequent photopatterning. Laminated dry photoresist is sold in between a layer of PET and polyolefin films to prevent contamination and facilitate handling. Prior to lamination to the PCB, the polyolefin layer is peeled off. PET layer is released before or after exposure. Both PET and polyolefin feature a low adhesion to the resist which allows for an easy, clean release.

square patterns on PET to act as substrate for the subsequent fabrication of SU-8 patterns (Fig. 10). The second approach was preferred since it allows the fabrication of structures within structures. The use of a SU-8 substrate improves the fidelity of SU-8 patterns to the design intended originally. Fig. 25 shows patterns exposed from similar blank disks on the mask and following the same process. The walls of the cylinder are intended to be vertical. As expected, results show how the use of a SU-8 substrate gives the best results (Fig. 25A ). Comparable results are obtained with Kapton® film substrates (Fig. 25B) as the CTE of polyimide approaches that of SU-8. However, the use of Cirlex®, a stack of polyimide films, gives the substrate a rigidity that negatively impacts wall verticality (Fig. 25C). The worst results are obtained with the use of silicon substrates (Fig. 25D). Therefore, the magnitude of the mismatch between the CTE of SU-8 and its substrate and the rigidness of the latter significantly impact SU-8 processing. The negative results obtained with a mismatch on the CTEs of the different materials in the mold are further amplified during pyrolysis as can be qualitatively concluded from Fig. 25 (right column). At the end, the use of SU-8 free standing mold precursors greatly improves carbon mold fidelity to the original design albeit the isometric carbon shrinkage.

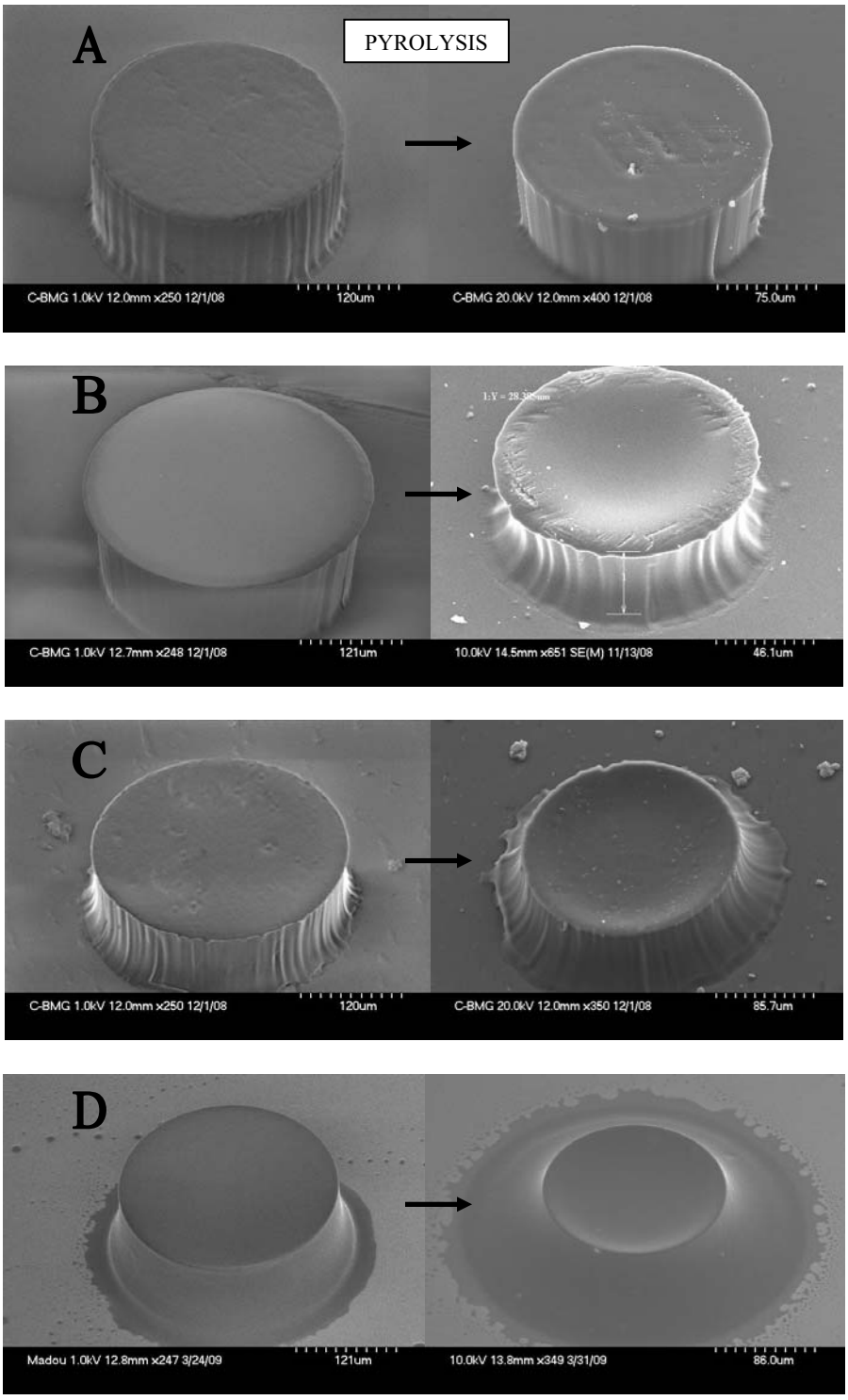


**Figure 25** SU-8 structures deformation due to thermal stresses when employing different substrates: A) SU-8, B) Kapton® film, C) Cirlex® and D) silicon wafer. Left column are SU-8 parts that are then carbonized by pyrolysis (shown in right column)

A BMG forming process using the molds derived from free standing SU-8 parts is shown in Fig. 26. The replication of even the slightest feature on the carbon mold is remarkable. Cleaning of the formed BMG gear was not conducted. The use of the all-carbon molds, derived from free standing SU-8 parts, allowed for better wall verticality than carbon-on-silicon or the all-carbon derived from SU-8 on polyimide substrates. However, the walls are still considerably rough and have a negative slope (<90 °C) that causes the mechanical interlock of the BMG part to the carbon mold and thus prevents a clean demolding step. Mechanical interlocking is demonstrated by the facts that the carbon mold, regardless of the type, is broken upon forcing the BMG part out (Fig. 22E, F) and that carbon residues are still present on the BMG walls even after oxygen plasma and sonication treatments (Fig. 19). Even when the surface roughness of the final BMG parts can be improved by re-heating above their glass transition temperature [24], smoother walls with a positive slope to eliminate mechanical locking were required. It was believed that the fulfilling of these requirements would enable a clean demolding process and render the cleaning by oxygen plasma step unnecessary, except of course when considering the use of sacrificial molds in certain applications. It is important to mention that glass-like carbon is well known for its inertness and near-atomically-flat surface and is routinely used as crucible material since most materials are incapable of wetting it.

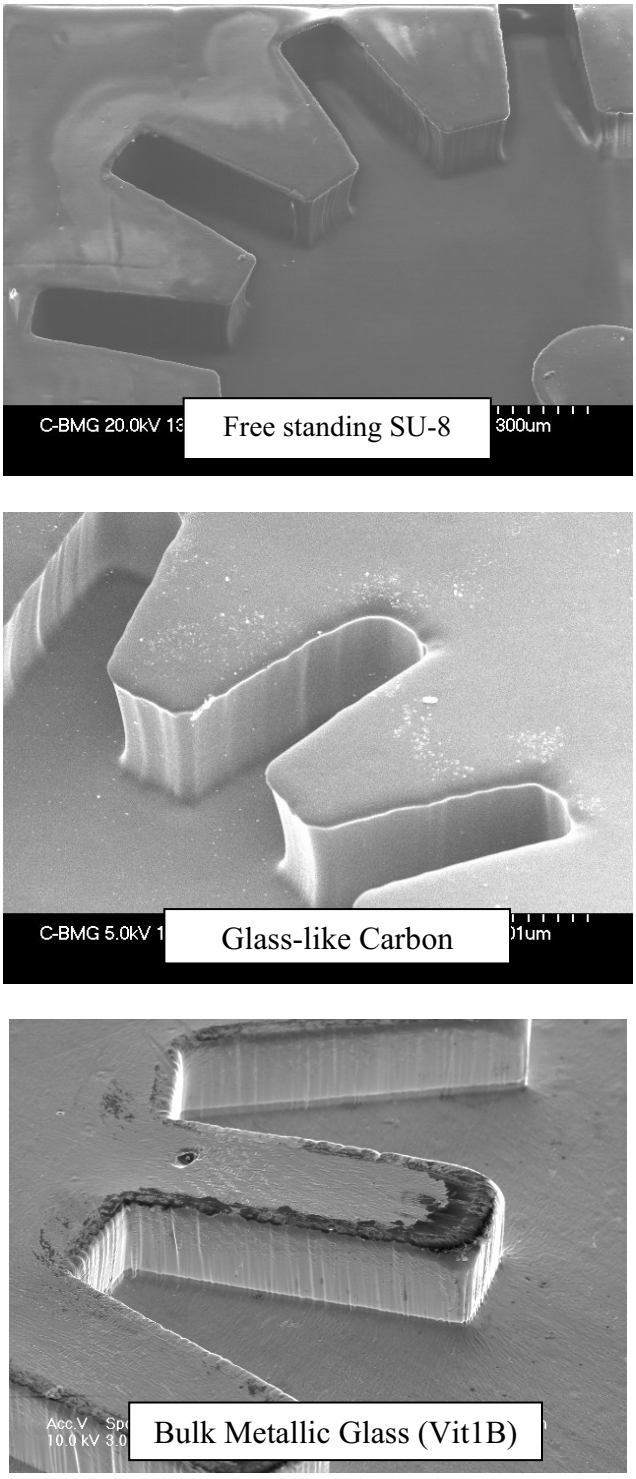


**Figure 26** BMG forming process using carbon molds derived from free standing SU-8

The next improvement, albeit a not so novel one, was the adoption of a high quality photomask instead of transparency mask. The new photomask consisted on a patterned chromium layer on a quartz plate. Patterning was done with e-beam lithography. Mask was fabricated at Tanner Research, Inc. (Monrovia, CA) and was facilitated by Dr. Jan Schroers from Yale University. Significantly smoother walls are obtained with the use of such mask. The results on SU-8 were already detailed in Chapter 2, Exposure section, Fig. 5. Carbon parts derived from such SU-8 molds are shown in Fig. 27.

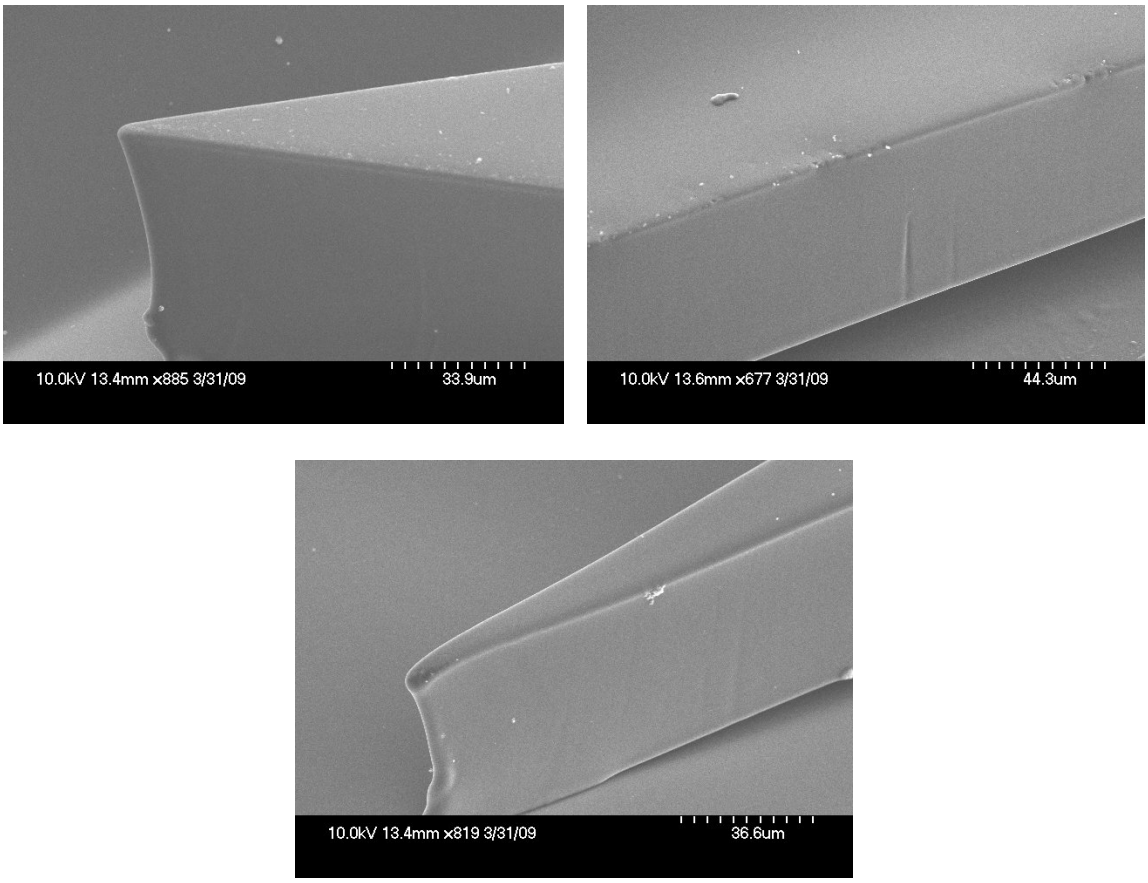


**Figure 27** Carbon molds with minimal surface roughness

The third major enhancement to the fabrication process was the capability to fabricate mold walls with positive slope using back-exposure of SU-8 through the transparent substrate. Again, the use of PET as substrate proved to be crucial. The details of this improvement were already discussed in Chapter 2. Even when this improvement can be easily implemented with any transparent substrate, glass or quartz for instance, the use of transparent films, such as PET, provides a flexible substrate which enables the clean release of the SU-8 mold from the film at the end of the process; a challenging action when using glass or quartz. Different SU-8 structures were derived with this approach and later carbonized. BMG molding and demolding are pending to be tested.

Summarizing, a series of improvements were incorporated to a traditional photolithography process to enable the fabrication of flat carbon molds that feature smooth walls with a positive slope. The first enhancement was the use of a PET film as a substrate that could be peeled from the SU-8 parts prior to pyrolysis. This allowed for free standing SU-8 molds. The use of a thick layer of SU-8 as a holding substrate for SU-8 patterns was proved to yield the best fidelity to the intended original design. Furthermore, the use of free standing SU-8 molds eliminated thermal stresses induced during pyrolysis and minimized distortion of the carbon structure with respect to the carbonization precursor. The second improvement was the adoption of an e-beam patterned chromium-on-quartz mask. This allowed for the obtainment of smooth walls in the carbon mold. The third improvement was the implementation of a back-exposure protocol through the transparent PET substrate. This yielded positive wall slopes in the mold.

Even when carbon molds possessing desired features were obtained by this work, their processing time was prohibitively long to enable an economically sound mass production. For example, the fabrication of carbon molds derived from 350 μm high SU-8 features patterned on a 100 μm thick SU-8 holding substrate took as long as 30.5 hours. Table 6 breaks down the process in the required steps and their time duration when fabricating molds with thicknesses between 200 and 400 μm. It can be seen that soft baking and carbonization are the lengthiest steps. Extended bake times were implemented to account for the fact that SU-8 develops a hard skin that hinders the efficient evaporation of solvent when using a convection oven. A hotplate could not be used as the PET substrate is an efficient heat attenuator. However, while the time for carbonization is not amenable for reducing, soft bake times are. The ideal case would be the complete elimination of the soft bake step. This single action would cut the fabrication time in half.

**Table 6** Fabrication process and time duration of each step

| Step | Time duration (in minutes) | % of total |
|---|---|---|
| Substrate preparation | 60 | **3** - *3.7* |
| SU-8 Substrate fabrication (100 μm thickness) | | |
| Spin Coating | 5 | **0.25** - *0.3* |
| Soft bake (in oven) | 120 | **6.1** - *7.5* |
| Exposure | 5 | **0.25** - *0.3* |
| PEB | 30 | **1.5** - *1.9* |
| Developing | 20 | **1** - *1.2* |
| SU-8 Patterns (200-400 μm thickness) | | |
| Spin Coating | 5 | **0.25** - *0.3* |
| Soft bake (in oven) | *600* - **960** | *37.8* - **49.35** |
| Exposure | 10 | **5.1** - *6.3* |
| PEB | 40 | **2** - *2.5* |
| Developing | 30 | **1.5** - *1.9* |
| Carbonization | 660 | **33.93** - *41.64* |
| TOTAL | *1585*-**1945** (*26.5* – **32. 5** h) | 100 |

Fig. 28 shows a suggested manufacturing line for the fabrication of free standing polymer molds. While SU-8 could be the photoresist of choice, several other materials could be used as long as they can be photopatterned. The first and most important step is the replacement of resist spin coating with lamination. Because photoresist is not needed to flow in order to be able to laminate it, soft bakes are no longer needed since no solvent must be evaporated. Photoresist formulations containing only the resist and its photoinitiator can be laminated above the glass transition temperature Tg of the resist (55 °C in the case of SU-8). Besides allowing for the elimination of soft bake steps, lamination brings a myriad of advantages when compared to spin coating. Achievable film thicknesses depend only on the pressure applied and separation between rollers in the lamination system and not on the viscosity of the photoresist or the capability of a

spin coater (maximum spin rate, acceleration rates, spin rate resolution). The obtainment of film thicknesses above 500 μm is significantly easier with lamination than with spin coating. Processing times prior to exposure are the same whether fabrication of 10 μm or 1 mm thick structures is conducted. The elimination of spin coating allows for the reduction on substrate preparation times and renders the use of fancy film holders, like the aluminum ones suggested, unnecessary. Nevertheless, lamination can be a continuous process while spin coating it is not. By replacing spin coating with lamination in the way suggested above, processing times of thick films are reduced in 50-60%. Laminated dry photoresists are available commercially. Some examples include Riston®, Ordyl BF 410, Etertec® 5600, DF 4615 and DFR-15. The biggest disadvantage of dry resist is its relatively low resolution compared to liquid resists. Two major reasons for this poorer resolution are the thicker resist coating and the fact that the mask is positioned on top of a thick protective cover film. By removing the top cover sheet from the photoresist prior to exposure, higher resolutions are possible.

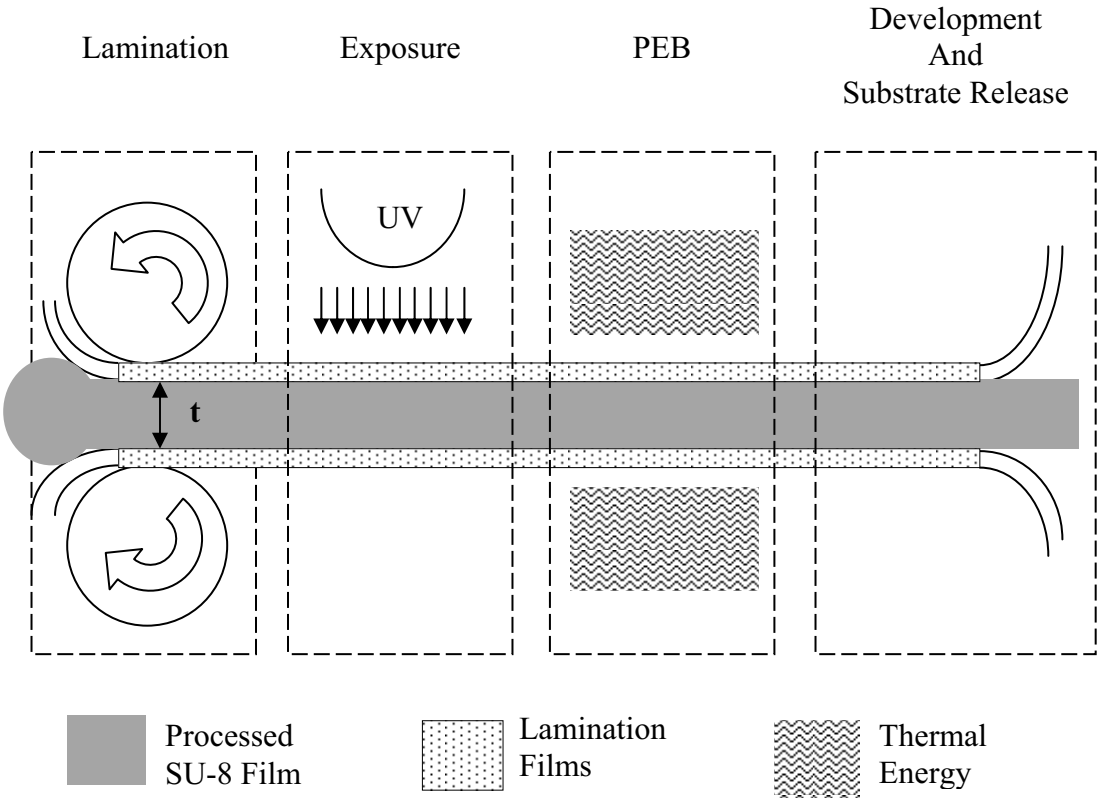


**Figure 28** Suggested manufacturing line for the fabrication of carbon molds

Once a polymer film with the desired thickness has been laminated, the polymer on PET film is positioned in a back-exposure system. A sequential exposure scheme as the one suggested in Fig. 11 is employed. The mask with the patterns of the mold is first exposed utilizing an energy dose capable of inducing sufficient cross-linking across the complete thickness of the film. The second mask contains the pattern to fabricate the holding substrate and is exposed with a dose corresponding to its desired thickness. The use of more sequential masks exposed with different dose, or a mask featuring different degrees of attenuation for different patterns, for *Grayscale Lithography* of the mold could be

incorporated as well. Intricate 3D patterns could also be achieved with the use of grayscale, or sequential, masks and exposure sources on both sides of the film (Fig. 29). Different thicknesses can be implemented by varying the dose each of the lamps delivers. Any of the above schemes: sequential mask exposure, grayscale masks or two-source exposure systems permits the fabrication of several layers of a mold in the same exposure step. Recall that lamination enables the use of very thick films. As an example, one could laminate a 1 mm layer, expose mold features and then use a dose to expose the holding substrate that yields a thickness of 100 μm. The use of proper masks and a back-exposure protocol yields the desired smooth, positive slope walls on the mold. Since high quality masks (chromium-on-quartz) are usually patterned with e-beam lithography, using a *software* mask, sequential masks to be exposed could be aligned at the whole-mask level (alignment between patterns of different masks can be done by aligning software masks used by the e-beam tool). The use of an SF-100 system (Chapter 2, Fig. 14 and 15) could be incorporated to benefit instant alignment between masks and the developing of grayscale structures. However, the exposure field size of such systems (~ 1 $cm^2$) reduces the production volume. The ultimate solution would be the use of electronic paper [127, 128] as photolithography mask. In its most basic version, electronic paper would allow for different software masks to be sequentially loaded to the electronic paper and get instantly and correctly aligned. More advanced versions would allow for the implementation of grayscales in the electronic mask. Electronic paper is now used in portable digital reader devices, also known as e-book reader or device, such as the Amazon Kindle™ or Sony's Reader Digital Books. Required improvements to be done to the technology are the obtaining of a transparent electronic paper, such that generates

patterns that either block or allow the passage of UV light, and the reduction of the resolution as current values, 0.1 to 5 μm, are not amenable to obtain the wall smoothness required for micro molds. Is important to note that current commercial UV sources are able to provide a collimated beam of light of up to 12" by 12" area and uniformity of +/- 6% [129].

After film has been exposed, post exposure bake (PEB) (if required) and developing are conducted in a normal way. Finally, polymer molds are peeled from the PET film and get carbonized in a traditional manner. The resultant manufacturing process for thick SU-8 films (200-400 um) is summarized in Table 7. Note how the process time is cut in more than half when compared to that of Table 6. The use of different photoresists would change the exposure, PEB and developing times but the elimination of soft bake and the high percentage that carbonization holds in the process would not be significantly changed.

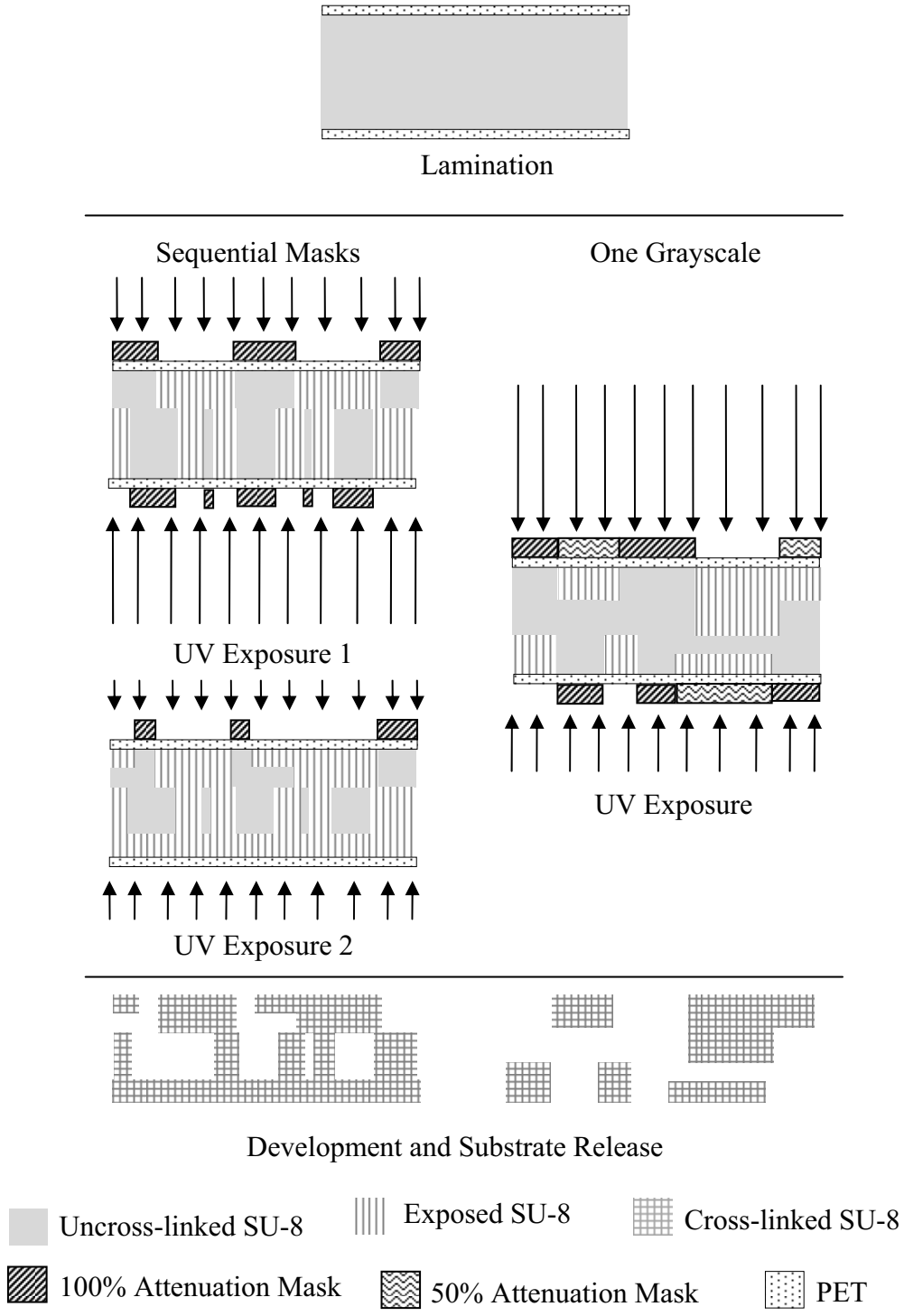


**Figure 29** A two-source illumination system for *Grayscale Lithography* using sequential masks (left) or a grayscale mask (right)

**Table 7** Suggested fabrication process and time duration of each step

| Step | Time (in minutes) | % of total |
|---|---|---|
| Lamination | continuous | |
| Exposure | 10 | 1.4 |
| Post exposure Bake (PEB) | 40 | 5.3 |
| Developing & Substrate Release | 40 | 5.3 |
| Carbonization | 660 | 88 |
| **TOTAL** | **750 (12.5 h)** | |

Further work is necessary to fully characterize achievable geometries, repeatability and dimensional tolerance ranges in the carbon molds when using the fabrication method developed in Chapters 2 and 3. BMG molding and demolding are pending to be characterized when using the improved carbon molds derived from free standing SU-8 parts. The molding of materials other than BMGs, for example the forming of glass micro lenses, is also planned to be tackled.

# CHAPTER 5. Nanomolding

The addition of Next-Generation Lithography (NGL) techniques, such as electron beam lithography (EBL), nanoimprint lithography (NIL) and focused-ion beam (FIB) will further reduce the dimensions and greatly increase the intricacy of the resulting carbon molds. The derivation of carbon molds with features in the nanoscale can be derived by the patterning of the precursor polymer, the direct patterning of a glass-like carbon piece or a combination of both. Moreover, nano-sized patterns could be fabricated in polymer or carbon structures that had already been micropatterned. The next sections give an overview on possible techniques that could be employed.

## *Electron Beam Lithography*

Direct write electron-beam lithography (EBL) or simply e-beam is a high-resolution patterning technique in which high-energy electrons (10–100 keV) are focused into a narrow beam and are used to expose electron-sensitive resists. Patterning resolutions down to 24 nm have been achieved with EBL and different resins [130, 131]. This technique is not suitable for the direct patterning of a carbon piece. There are two basic ways to scan an electron beam. In raster scanning, the patterns are written by an electron beam that moves through a regular pattern. The beam scans sequentially over the entire area and is blanked off where no exposure is required. On the contrary, in vector scanning, the electron beam is directed only to the requested pattern features and hops from features to features. Time is therefore saved in a vector scan system. The diffraction

effects that often cause a slope on walls fabricated with photolithography are not an issue in EBL because the quantum mechanical wavelengths of high-energy electrons are exceedingly small. Because of its serial nature, the use of electron-beam lithography has been limited to mask making and direct writing on wafers for specialized applications.

Nanomolds could be fabricated by patterning nanostructures on SU-8, PMMA or any other suitable resist[131] for subsequent carbonization. Free standing molds could be fabricated in the same manner they were derived above, namely fabricating a polymer holding substrate and patterning a film on top of them. PET film is then released prior to pyrolysis.

### *Focused Ion Beam*

As its name implies, in Focused Ion Beam lithography (FIB) the work-piece is exposed to a focused and highly energetic ion bombardment in a vacuum. FIB lithography, sometimes also known as FIB milling, consists of point-by-point exposures with a narrow ion beam generated by a source of liquid metal (usually gallium) and is capable of milling carbon among several other materials. The kinetic energy of the ions ranges from a few keV up to several MeV. Beam diameters of less than 50 nm and current densities up to 8 $A/cm^2$ are the norm. In addition to gallium, other pure element sources are available including indium and gold. Compared to photons (x-rays and DUV light) or electrons (EBL), ions chemically react with the substrate, allowing for a greater variety of surface modifications such as patterned doping. The ion-beam spot size is the smallest possible, smaller than UV, x-ray, or electron-beam spots. Resolution achieved with FIB

can be as low as 3 nm [132] but normal values are around 8-10 nm [133, 134]. Ion lithography achieves higher resolution than optical, x-ray, or electron beam techniques because ions undergo almost no diffraction and scatter much less than electrons, since the secondary electrons produced by an ion beam are of lower energy and have a short diffusion range. The total spread including forward and backward scattering of the "stiffer" ion-beams is typically less than 10 nm and they only require about 1 to 10% of the electron dose to expose a resist. FIB shares the same drawbacks with an electron-beam system in that it requires a serially-scanned beam and a high vacuum. Because FIB systems operate in a similar fashion to a scanning electron microscope (SEM) they can be used for imaging (when operated at low beam currents) or for site specific sputtering or milling (when operated at high beam currents).

FIB milling has been employed recently for the patterning of bulk glass-like carbon. The resultant structures are used for the molding of borosilicate glasses and quartz [16, 135, 136]. A comparison between FIB, laser and mechanical milling for the patterning of carbon is given in [17, 18].

### *Nanodroplet Sputtering*

An alternative to FIB milling is the use of electrospray in vacuum to generate a focused beam of energetic nanodroplets for physical sputtering. This apparatus is currently being developed by Prof. Manuel Gamero-Castaño [137, 138] here at UC Irvine. The author of this thesis and Gamero-Castaño are currently evaluating the potential of such system for the patterning of glass-like carbon. 5-7 $mm^2$ squares of glass-like carbon were derived

from 1 $cm^2$ SU-8 and Kapton® squares. In the case of SU-8 derived carbon, samples were fabricated following the PET approach detailed in Chapter 2. In the case of polyimide, a commercially available Kapton® film was cut into the mentioned squares and then carbonized together with SU-8 squares in a process similar to that explained above. Glass-like carbon pieces featured a thickness >100 μm. It was qualitatively observed that polyimide has both better carbon yield and shrinkage behavior (it shrinks less) than SU-8. Such visualization suggested a higher carbon density in polyimide that in SU-8.

Electrospray refers to the atomization of liquids in the cone-jet mode which generates narrow droplet distributions with average diameters as small as a few nanometers [137, 139]. Electrospray generation depends on the value of an extraction voltage that gets applied between an emitter and an extracting electrode and causes the breakup of a jet into nanodroplets. Such phenomenon can be accurately described by the theory of capillary instability. In this system the fluid comes out from an approximated point source (emitter) at a set flow rate and gets shaped into a Taylor cone [140] by the applied voltage between the emitter and extractor electrodes. Nanodroplets are generated at the apex of the Taylor cone. An electrospray generated under vacuum features a narrower beam than those achieved by systems working under atmospheric pressure. Further narrowing of the beam can be achieved by the use of a skimmer, or an orifice in the extractor electrode, and optimization of the extraction voltage [137]. Preliminary results on the milling of glass-like carbon using nanodroplet sputtering have been promising. Holes of different depth and hundreds of micrometers in diameter were fabricated on carbon by varying the extraction voltage of the drops and keeping their diameter constant.

Characterization of the etch rate and surface polishing depending on the working parameters is pending to be done. Current etch rates compare to the 1.2 μm/min obtained with ICP/RIE (Chapter 3).

The possible use of nanodroplet sputtering over FIB would derive in lower process cost since no liquid metal sources are necessary. The replacement of liquid metals by more environmentally friendly liquids is also an advantage. Nevertheless, it has been shown before that carbon molds obtained with FIB milling get affected by gallium ion implantation that might require the use of high temperature treatments (1400 °C) to eliminate [16]. Nanodroplet sputtering does not generate any implanted ions. However, the capabilities of nanodroplet sputtering still have to be proven.

### *Nano Imprint Lithography*

Nano Imprint lithography (NIL) [141-143] patterns a substrate material by deforming its shape through embossing (with a mold/stamp/template), rather than by altering the material's chemical, through radiation, or physical structure through sputtering. Embossing must be done preferably above the glass transition temperature of the substrate material. NIL has been extensively demonstrated in resists and other polymers and has been recently achieved in BMGs [125]. In NIL, a template (the mold/stamp/template) is made of a hard material (usually Ni or Si) and is pressed against a layer of a suitable material. Logically, the mold/stamp/template must maintain its structural integrity at temperatures and pressures well above the imprinting conditions. The method relies on the excellent replication fidelity obtained with polymers and

materials featuring a glassy state and combines thermo-plastic molding with common pattern transfer methods. Once a solid mold/stamp with a nano-relief on its surface is fabricated it can be used for the replication of many identical surface patterns. Since the resolution of the NIL process is a direct function of the resolution of the original template/stamp fabrication process it does not technically fall into the definition of a NGL. However, is an efficient process for the mass production of nano-featured parts, an accomplishment none of the other NGL techniques has been able to achieve. Electron beam writers that provide high resolution, but lack the throughput required for mass production, are usually employed for the fabrication of the mold/stamps. Other techniques, such as FIB and maybe eventually nanodroplet sputtering, could also be used for the fabrication of the molds. The success of NIL proves the fact that molding/embossing are some of the best ways to achieve mass production of a part regardless of its dimensions.

As expected, the derivation of carbon nanomolds with NIL is most likely achieved by patterning an organic polymer and carbonizing. The author believes glass-like carbon would be better exploited in NIL as a mold/stamp material given its outstanding thermal, mechanical and chemical properties. Namely, the very high melting temperature and material hardness make glass-like carbon a candidate comparable, or maybe better, to Ni or Si. Carbon nanomolds obtained with any of the techniques above could be used to further produce carbon nanomolds in mass by imprinting polymers and carbonize them after. The fact that the resultant carbon structure is smaller than the polymer precursor can be exploited to obtain an ever-smaller carbon mold as the number of molding cycles

increases. For instance, a carbon mold can be fabricated either by patterning a polymer with e-beam (30 nm resolution) or by patterning a carbon piece by FIB (10 nm). In the case of e-beam, the polymer precursor is pyrolyzed to obtain a carbon mold that is smaller than the polymer one. The resultant carbon mold from the e-beam or FIB process can then be used to pattern a polymer with NIL with features of 10-20 nm. That patterned polymer is then carbonized to obtain carbon molds with reduced dimensions and so on. Pattern dimensions smaller than those currently achieved by FIB or e-beam could be obtained. Theoretically, the process could be carried until the physical limit of available carbon molecules and rings is reached. This approach has been successfully demonstrated in the micron range by [144].

# CHAPTER 6. Conclusions

A novel method to derive free standing glass-like carbon molds has been obtained in this work. The use of such molds has been demonstrated with the forming of amorphous metal in different shapes and dimensions, including high aspect ratio features. Carbon molds were derived through the pyrolysis of patterned SU-8 parts that were fabricated using an improved photolithography process. Such enhancements to the traditional photolithography process allowed for the derivation of carbon molds featuring smooth walls with positive slopes. Resultant carbon molds comply with the mechanical and thermal integrity of a permanent mold and yet are fabricated at a cost that enables their potential use as sacrificial molds. For this purpose, carbon etching with oxygen plasma was also demonstrated. Pending work includes the characterization of the process in terms of achievable geometries and dimensions, shrinkage behavior and reproducibility.

The developed process has the potential to become an alternative to LIGA for the derivation of permanent molds featuring high-aspect-ratios. The main difference is that the derivation of carbon micro molds does not employ electroplating, but only photolithography and carbonization, which reduces the cost of the process. Furthermore, the capability of BMG forming with the fabricated carbon molds enables the use of micro molded BMG parts for different applications.

In order to promote the mass production of carbon micro molds, a manufacturing line was also suggested. This fabrication approach allowed for a theoretical time reduction of more than half when compared to the current process and is amenable for automation.

Different techniques were explored and considered as potential candidates for the fabrication of nanomolds or for the fabrication of intricate features on existent micro molds. These techniques included EBL, FIB, Nanodroplet sputtering and NIL. Of most interest is the concept of continuous reduction of the critical dimension by exploiting the isometric shrinkage present during the pyrolysis of organic polymers. In this way, structures with the minimal dimension currently achieved by EBL or FIB could be patterned in polymer and get carbonized thereafter. The resultant carbon structure features a smaller critical dimension than its polymer precursor and possesses mechanical properties that allow its use as a mold/stamp in NIL. This fact is exploited for the stamping of a polymer, and its respective carbon structure after pyrolysis, and for the obtainment of an ever-smaller critical dimension as the number of cycles increases.

## REFERENCES

[1] Weber L, Ehrfeld W, Freimuth H, Lacher M, Lehr H and Pech B (1996) Micro molding - a powerful tool for the large scale production of precise microstructures. In Proc SPIE: Austin TX, October 14, 1996. 2879:156-167

[2] Yu L, Koh CG, Lee LJ, Koelling KW and Madou MJ (2002) Experimental investigation and numerical simulation of injection molding with micro-features. Polymer Engineering and Science 42:871-888

[3] Knights M (2002) Micro molds make micro parts. Plastics Technology 48:38-43

[4] Griffiths CA, Dimov SS, Brousseau EB and Hoyle RT (2007) The effects of tool surface quality in micro-injection moulding. J.Mater.Process.Technol. 189:418-427

[5] Peng Z, Gang L, Yangchao T and Xuehong T (2005) The properties of demoulding of Ni and Ni-PTFE moulding inserts. Sensors and Actuators A: Physical 118:338-341

[6] Choi W, Lee J, Kim W, Min B, Kang S and Lee S (2004) Design and fabrication of tungsten carbide mould with micro patterns imprinted by micro lithography. J Micromech Microeng 14:1519-1525

[7] Lim HS, Wong YS, Rahman M and Edwin Lee MK (2003) A study on the machining of high-aspect ratio micro-structures using micro-EDM. J.Mater.Process.Technol. 140:318-325

[8] Nakamoto T, Yamaguchi K, Abaraha PA and Mishima K (1996) Manufacturing of three-dimensional micro-parts by UV laser induced polymerization. J Micromech Microeng 6:240-253

[9] Fleischer J and Kotschenreuther J (2007) The manufacturing of micro molds by convential and energy-assisted processes. Int J Adv Manuf Technol 33:75-85

[10] Giboz J, Copponnex T and Mélé P (2007) Microinjection molding of thermoplastic polymers: a review. J Micromech Microeng 17:R96-R109

[11] Heckele M and Schomburg WK (2004) Review on micro molding of thermoplastsic polymers. J Micromech Microeng 14:R1-R14

[12] Piotter V, Holstein N, Plewa K, Ruprecht R and Hausselt J (2004) Replication of micro components by different variants of injection molding. Microsystems Technologies 10:547-551

[13] Ranganathan S and McCreery RL (2001) Electroanalytical Performance of Carbon Films with Near-Atomics Flatness. Anal Chem 73:893-900

[14] Angle MA, Blair GE and Maier CC (1974) Method for molding glass lenses.3833347

[15] Angle ME, Bender GL, Blair GE and Maier CC (1974) Method and Apparatus for Transfer Molding Glass lenses.3844755

[16] Youn SW, Takahashi M, Goro H and Maeda R (2006) A study on focused ion beam milling of glassy carbon molds for the thermal imprinting of quartz and borosilicate glasses. J Micromech Microeng 16:2576-2584

[17] Youn SW, Takahashi M, Goto H and Maeda R (2006) Microstructuring of glassy carbon mold for glass embossing – Comparison of focused ion beam, nano/femtosecond-pulsed laser and mechanical machining. Microelectronic Engineering 83:2482-2492

[18] Youn SW, Takahashi M, Goto H and Maeda R (2007) Fabrication of micro-mold for glass embossing using focused ion beam, femto-second laser, eximer laser and dicing techniques. J.Mater.Process.Technol. 187-188:326-330

[19] Schroers J and Paton N (2006) Amorphous metal alloys form like plastics. Adv Materials & Proc 164:61-63

[20] Schroers J, Pham Q and Desai A (2007) Thermoplastic Forming of Bulk Metallic Glass - A Technology for MEMS and Microstructure Fabrication. J MEMS 16:240-247

[21] Schroers J, Veazey C and Johnson WL (2003) Amorphous metallic foam. Appl Phys Lett 82:370-372

[22] Schroers J, Pham Q, Peker A, Paton N and Curtis RV (2007) Blow molding of bulk metallic glass. Scr.Mater. 57:341-344

[23] Saotome Y, Imai K, Shioda S, Shimizu S, Zhang T and Inoue A (2002) The micro-nanoformability of Pt-based metallic glass and the nanoforming of three-dimensional structures. Intermetallics 10:1241-1247

[24] Kumar G and Schroers J (2008) Write and erase mechanisms for bulk metallic glass. APL 92:031901-0-031901-3

[25] Dobbs HS (1974) Vitreous Carbon and the brittle fracture of amorphous solids. J Phys D: Appl Phys 7:24-34

[26] Bragg RH and Hammond ML (1965) X-ray study of pyrolytic graphites and glassy carbons. Carbon 3:340-340

[27] Rothwell WS (1968) Small-angle X-Ray Scattering from Glassy Carbon. J Appl Phys 39:1840-1845

[28] McFeely SP, Kowalczyk SP, Ley L, Cavell RG, Pollak RA and Shirley DA (1974) X-ray photoemission studies of diamond, graphite, and glassy carbon valence bands. Phys Rev B 9:5268-5278

[29] Nishikawa K, Fukuyama K and Nishizawa T (1998) Structure Change of Glass-like Carbon with Heat Treatment, Studied by Small Angle X-Ray Scattering: I. Glass-like Carbon Prepared from Phenolic Resin. Jpn J Appl Phys 37:6486-6491

[30] Fukuyama K, Nishizawa T and Nishikawa K (2001) Investigation of the pore structure in glass-like carbon prepared from furan resin. Carbon 39:2017-2021

[31] Iwashita N, Park CR, Fujimoto H, Shiraishi M and Inagaki M (2004) Specification for a standard procedure of X-ray diffraction measurements on carbon materials. Carbon 42:701-714

[32] Dekanski A, Stevanovic J, Stevanovic R, Nikolic BZ and Jovanovic VM (2001) Glassy carbon electrodes: I. Characterization and electrochemical activation. Carbon 39:1195-1205

[33] Oberlin A and Oberlin M (1983) Graphitizability of carbonaceous materials as studied by TEM and X-ray diffraction. J Microscopy 132:353-363

[34] Hull R (1999) Properties of Crystalline Silicon. The Institution of Engineering and Technology, London

[35] Lide DR (1992) Handbook of Chemistry and Physics. CRC Press, Boca Raton, FL

[36] Yamada S and Sato H (1962) Some Physical Properties of Glassy Carbon. Nature 193:261-262

[37] Lewis JC, Redfern B and Cowlard FC (1963) Vitreous carbon as a crucible material for semiconductors. Sol State Electron 6:251-254

[38] Cowlard FC and Lewis JC (1967) Vitreous Carbon - A New Form of Carbon. J Mat Sci 2:507-512

[39] Cahn W and Harris B (1969) Newer Forms of Carbon and their Uses. Nature 221:132-141

[40] Halpin MK and Jenkins GM (1969) Interaction of glassy carbon with alkali metal vapours. Proc Roy Soc Lond A 313:421-431

[41] Jenkins GM and Kawamura K (1976) Polymeric Carbon - Carbon Fibre, Glass and Char. Cambridge University Press, London, New York

[42] Jenkins GM, Kawamura K and Ban LL (1972) Formation and Structure of Polymeric Carbons. Proc of the Royal Soc of London, Series A 327:501-517

[43] Kakinoki J (1965) A model for the structure of 'glassy carbon'. Acta Cryst 18:578-578

[44] Jenkins GM and Kawamura K (1971) Structure of Glassy Carbon. Nature 231:175-176

[45] Pesin LA (2002) Structure and Properties of glass-like carbon. J Mat Sci 37:1-28

[46] Shiraishi M (1984) Kaitei Tansozairyo Nyumon (Introduction to Carbon Materials). Tanso Zairyo Gakkai 29-33

[47] Fedorov VB, Shorshorov MK and Khakimova DK (1978) Carbon and its Interaction with Metals. Metalurgiya

[48] Spain IL(1981) The Electronic Transport Properties of Graphite, Carbons, and Related Materials. In: Walker Jr. PL and Thrower PA (ed) Chemistry and Physics of Carbon, Marcel Dekker, Inc., New York

[49] Weintraub E and Miller LB (1915) Microphone.1156509

[50] Redfern B and Greens N (1963) Bodies and Shapes of Carbonaceous Materials and Processes for their Production.US 3109712

[51] Davidson HW (1962) Nucl Engng 7:159

[52] Benson J (1969) Carbon offers advantages as implant material in human body. NASA Technical Brief

[53] Benson J (1971) Elemental Carbon as a Biomaterial. J Biomed Mat Res 5:41-47

[54] Von Fraunhofer JA, L'estrange PR and Mack AO (1971) Materials science in dental implantation and a promising new material: vitreous carbon. Biomed Eng 6:114-118

[55] http://www.tokaicarbon.co.jp/en/products/fine_carbon/gc.html . Accessed on 05/12, 2009.

[56] Schueller OJA, Brittain ST and Whitesides GM (1997) Fabrication of Glassy Carbon Microstructures by Pyrolysis of Microfabricated Polymeric Precursors. Adv Mat 9:477-480

[57] Schueller OJA, Brittain ST, Marzolin C and Whitesides GM (1997) Fabrication and Characterization of Glassy Carbon MEMS. Chemistry of Materials 9:1399-1406

[58] Schueller OJA, Brittain ST and Whitesides GM (1999) Fabrication of glassy carbon microstructures by soft lithography. Sensors and Actuators A: Physical 72:125-139

[59] Schueller OJA, Brittain S and Whitesides GM (2000) Fabrication of Carbon Microstructures.6143412

[60] Zhao X, Xia Y, Schueller OJA, Qin D and Whitesides GM (1998) Fabrication of microstructures using shrinkable polystyrene films. Sensors and Actuators A: Physical 65:209-217

[61] Kim J, Song X, Kinoshita K, Madou M and White R (1998) Electrochemical Studies of Carbon Films from Pyrolyzed Photoresist. J Electrochem Soc 145:2314-2319

[62] Ranganathan S, McCreery RL, Majji SM and Madou M (2000) Photoresist-Derived Carbon for Microelectromechanical Systems and Electrochemical Applications. J Electrochem Soc 147:277-282

[63] Kostecki R, Song X and Kinoshita K (2000) Influence of Geometry on the Electrochemical Response of Carbon Interdigitated Microelectrodes. J Electrochem Soc 147:1878-1881

[64] Lorenz H, Despont M, Fahrni M, LaBianca N, Vettiger P and Renaud P (1997) SU-8: a low-cost negative resist for MEMS. J Micromec Microeng 7:121

[65] Shaw JM, Gelorme JD, LaBianca NC, Conley WE and Holmes SJ (1997) Negative photoresists for optical lithography. IBM J Res Dev 41:81-94

[66] Singh A, Jayaram J, Madou M and Akbar S (2002) Pyrolysis of Negative Photoresists to Fabricate Carbon Structures for Microelectromechanical Systems and Electrochemical Applications. J Electrochem Soc 149:E78-E83

[67] Wang C, Jia G, Taherabadi LH and Madou MJ (2005) A Novel Method for the Fabrication of High-Aspect Ratio C-MEMS Structures. J of MEMS 14:348-358

[68] Wang C and Madou M (2005) From MEMS to NEMS with carbon. Biosens and Bioelectron 20:2181-2187

[69] Park BY, Taherabadi L, Wang C, Zoval J and Madou MJ (2005) Electrical Properties and Shrinkage of Carbonized Photoresist Films and the Implications for Carbon Microelectromechanical Systems Devices in Conductive Media. J Electrochem Soc 152:J136-J143

[70] Malladi K, Wang C and Madou M (2006) Fabrication of suspended carbon microstructures by e-beam writer and pyrolysis. Carbon 44:2602-2607

[71] Wang C, Taherabadi L, Jia G, Madou M, Yeh Y and Dunn B (2004) C-MEMS for the Manufacture of 3D Microbatteries. Electrochem Solid-State Lett 7:A435-A438

[72] Galobardes F, Wang C and Madou M (2006) Investigation on the solid electrolyte interface formed on pyrolyzed photoresist carbon anodes for C-MEMS lithium-ion batteries. Diamond and Related Materials 15:1930-1934

[73] Min H, Park BY, Taherabadi L *et al.* (2008) Fabrication and properties of a carbon/polypyrrole three-dimensional microbattery. J.Power Sources 178:795-800

[74] Teixidor GT, Zaouk RB, Park BY and Madou MJ (2008) Fabrication and characterization of three-dimensional carbon electrodes for lithium-ion batteries. J.Power Sources 183:730-740

[75] Park BY and Madou MJ (2006) Design, fabrication, and initial testing of a miniature PEM fuel cell with micro-scale pyrolyzed carbon fluidic plates. J.Power Sources 162:369-379

[76] Lin P, Park BY and Madou MJ (2008) Development and characterization of a miniature PEM fuel cell stack with carbon bipolar plates. J.Power Sources 176:207-214

[77] Xu H, Malladi K, Wang C, Kulinsky L, Song M and Madou M (2008) Carbon post-microarrays for glucose sensors. Biosensors and Bioelectronics 23:1637-1644

[78] Turon Teixidor G, Gorkin III RA, Tripathi PP *et al.* (2008) Carbon microelectromechanical systems as a substratum for cell growth. Biomed Mater 3:034116

[79] Park BY and Madou MJ (2005) 3-D electrode designs for flow-through dielectrophoretic systems. Electrophoresis 26:3745-3757

[80] Martinez-Duarte R, Rouabah HA, Green NG, Madou M and Morgan H (2007) Higher Efficiency and Throughput in Particle Separation with 3D Dielectrophoresis with C-MEMS. In Proceedings of uTAS 2007: Paris, France, Oct. 7-11, 2007. 1:826-828

[81] Martinez-Duarte R, Andrade-Roman J, Martinez SO and Madou MJ (2008) A High Throughput Multi-stage, Multi-frequency Filter and Separation Device based on Carbon Dielectrophoresis. In Proceedings of NSTI Nanotech 2008: Boston, MA, June 1-5, 2008. 3:316-319

[82] Martinez-Duarte R, Cito S, Collado-Arredondo E, Martinez SO and Madou M (2008) Fluido-dynamic and Electromagnetic Characterization of 3D Carbon Dielectrophoresis with Finite Element Analysis. In Proceedings of NSTI Nanotech 2008: Boston, MA, 2008. 3:265-268

[83] Martinez-Duarte R, Cito S, Collado-Arredondo E, Martinez SO and Madou MJ (2008) Fluido-dynamic and Electromagnetic Characterization of 3D Carbon Dielectrophoresis with Finite Element Analysis. Sens and Transd J 3:25-36

[84] Martinez-Duarte R, Gorkin R, Abi-Samra K and Madou MJ (2009) The Integration of 3D Carbon Dielectrophoresis on a Rotating Platform. In Proceedings of Transducers 2009: Denver, CO, June 21-25, 2009. 2147-2150

[85] Madou MJ, Park BY and Paradiso AC (2006) Method and Apparatus for Dielectrophoretic Separation.US 2006/0260944A1

[86] Park BY, Zaouk R and Madou M (2004) Validation of lithography based on the controlled movement of light-emitting particles. In Proc of SPIE: 2004. 5374:566-578

[87] Martinez-Duarte R, Madou MJ, Kumar G and Schroers J (2009) A Novel Method for Amorphous Metal Micromolding using Carbon MEMS. In Proc of Transducers 2009: June 21- 25, 2009, 2009. 188-191

[88] Park BY, Zaouk R, Wang C and Madou MJ (2007) A Case for Fractal Electrodes in Electrochemical Applications. J Electrochem Soc 154:P1-P5

[89] Sharma CS, Kulkarni MM, Sharma A and Madou M (2009) Synthesis of carbon xerogel particles and fractal-like structures. Chemical Engineering Science 64:1536-1543

[90] Jeong OC and Konishi S (2008) Three-dimensionally combined carbonized polymer sensor and heater. Sens and Actuators A 143:97-105

[91] Ito H (1996) Chemical Amplification Resists: history and Development within IBM. IBM J Res & Dev 41:69-80

[92] Gelorme JD, Cox RJ and Gutierrez SAR (1989) Photoresist Composition and Printed Circuit Boards and Packages made therewith.4882245

[93] Angelo R, Gelorme J, Kucynski J, Lawrence W, Pappas S and Simpson L (1992) Photocurable epoxy composition with sulfonium salt photoinitiator.5102772

[94] Harris TW (1976) Chemical Milling. Clarendon Press, Oxford

[95] del Campo A and Greiner C (2007) SU:8 a photoresist for high-aspect-ratio and 3D submicron lithography. J Micromech Microeng 17:R81-R95

[96] www.microchem.com . Accessed on 04/12, 2009.

[97] http://www2.dupont.com/Kapton/en_US/ . Accessed on 04/15, 2009.

[98] http://www.matweb.com . Accessed on 04/15, 2009.

[99] http://usa.dupontteijinfilms.com/informationcenter/technicalinfo.aspx . Accessed on 04/16, 2009.

[100] http://memscyclopedia.org/su8.html . Accessed on 04/15, 2009.

[101] Metz TE, Savage RN and Simmons HO (1992) In Situ Control of Photoresist Coating Processes. Semicond Int 15:68-69

[102] Thompson LF(1994) An Introduction to Lithography. In: Thompson LF, Willson CG and Bowden MJ (ed) Introduction to Microlithography, Second edn. American Chemical Society, Washington, D. C.

[103] Fitzer E, Kochling KH, Boehm HP and Marsh H (1995) Recommended Terminology for the Description of Carbon as a Solid. Pure & Appl Chem 67:473-506

[104] Fitzer E, Schaefer W and Yamada S (1969) The formation of glasslike carbon by pyrolysis of polyfurfuryl alcohol and phenolic resin. Carbon 7:643

[105] Vohler O, Reiser P, Martina R and Ovrehoff D (1970) New forms of Carbon. Angewandte Chemie International in English 9:414-425

[106] Kawamura K and Kimura S (1983) Glass-like Carbon Made from Epoxy Resin Cured with 2, 4, 6-Trinitrophenol. Bull Chem Soc Jpn 56:2499-2503

[107] Aggarwal RK, Bhatia G, Bahl OP and Malik M (1988) Development of glass-like carbon from phenol formaldehyde resins employing monohydric and dihydric phenols. J Mat Sci 23:1677-1684

[108] Callstrom MR, Neenan TX, McCreery RL and Alsmeyer DC (1990) Doped glassy carbon materials (DGC): low-temperature synthesis, structure, and catalytic behavior. J.Am.Chem.Soc. 112:4954-4956

[109] Neenan TX, Callstrom MR, Bachman BJ, McCreery RL and Alsmeyer DC (1990) Doped Glassy Carbon Materials (DGC): Their Synthesis from Polymeric Precursors and Investigation of Their Properties. British Poly J 23:171-177

[110] Hutton HD, Huang W, Alsmeyer DC *et al.* (1993) Synthesis, characterization, and electrochemical activity of halogen-doped glassy carbon. Chemistry of Materials 5:1110-1117

[111] Shah HV, Brittain ST, Huang Q, Hwu S-, Whitesides GM and Smith DW (1999) Bis-o-diynylarene (BODA) Derived Polynaphthalenes as Precursors to Glassy Carbon Microstructures. Chemistry of Materials 11:2623-2625

[112] Hishiyama Y, Igarashi K, Kanaoka I *et al.* (1997) Graphitization behavior of Kapton-derived carbon film related to structure, microtexture and transport properties. Carbon 35:657-668

[113] Lee L (1965) Mechanisms of Thermal Degradation of Phenolic Condensation Polymers. II. Thermal Stability and Degradation Schemes of Epoxy Resins. J of Polymer Sci: Part A 3:859-882

[114] Fitzer E and Schafer W (1970) The effect of cross-linking on the Formation of Glasslike Carbons from Thermosetting Resins. Carbon 8:353-364

[115] Gac NA, Spokes GN and Benson SW (1970) Thermal Degradation of Nadic Methyl Anhydride-Cured Epoxy Novolac. J Poly Sci A 8:593-608

[116] Jenkins GM, Kawamura K and Ban LL (1972) Formation and Structure of Polymeric Carbons. Proc Roy Soc Lon A 327:501-517

[117] Lyons AM, Wilkins CW and Robbins M (1983) Thin pinhole-free Carbon films. Thin Solid Films 103:333-341

[118] Nakagawa H and Tsuge S (1987) Studies on Thermal Degradation of Epoxy Resins by High-Resolution Pyrolysis-Gas Chromatography. J Anal Appl Pyrolysis 12:97-113

[119] Chen KS and Yeh RZ (1996) Pyrolysis kinetics of epoxy resin in a nitrogen atmosphere. J Hazard Mat 49:105-113

[120] Beyler CL and Hirschler MM(2002) Thermal Decomposition of Polymers. In: Anonymous (ed)

[121] Ma CM, Chen C, Kuan H and Chang W (2004) Processability, Thermal, Mechanical, and Morphological Properties of Novolac Type-Epoxy Resin-Based Carbon-Carbon Composite. J Comp Mat 38:311-322

[122] Mehrotra BN, Bragg RH and Rao AS (1983) Effect of heat treatment temperature (HTT) on density, weight and volume of glass-like carbon (GC). J Mat Sci 18:2671-2678

[123] Johnson WL (2002) Bulk amorphous metal - An emerging engineering material. JOM 54:40-43

[124] Telford M (2004) The case for bulk metallic glass. Materials Today 7:36-43

[125] Kumar G, Tang H and Schroers J (2009) Nanomoulding with amorphous metals. Nature 7231:868-872

[126] Kuhnke M, Lippert T, Scherer GG and Wokaun A (2005) MicroFabrication of flow field channels in glassy carbon by a combined laser and reactive ion etching process. Surface and Coatings Technology 200:730-733

[127] Comiskey B, Albert JD, Yoshizawa H and Jacobson J (1998) An electrophoretic ink for all-printed reflective electronic displays. Nature 394:253-255

[128] Hayes RA and Feenstra BJ (2003) Video-speed electronic paper based on electrowetting. Nature 425:383-385

[129] http://www.tamsci.com/products/uvlighsrc.html . Accessed on 05/08, 2009.

[130] Bilenberg B, Jacobsen S, Schmidt MS *et al.* (2006) High resolution 100 kV electron beam lithography in SU-8. Microelectronic Engineering 83:1609-1612

[131] Robinson APG, Zaid HM, Gibbons FP *et al.* (2006) Chemically amplified molecular resists for electron beam lithography. Microelectronic Engineering 83:1115-1118

[132] Gierak J, Madouri A, Biance AL *et al.* (2007) Sub-5 nm FIB direct patterning of nanodevices. Microelectronic Engineering 84:779-783

[133] Volkert CA and Minor AM (2007) Focused Ion Beam Microscopy and Micromachining. MRS Bulletin 32:389-399

[134] Madou MJ (2009) Manufacturing Techniques for Microfabrication and Nanotechnologgy. CRC Press, Boca Raton, FL

[135] Youn SW, Takahashi M, Goto H, Kobayashi T and Maeda R (2006) The effect of heat-treatment conditions on mechanical and morphological properties of a FIB-milled glassy carbon mold with micro patterns. J Micromech Microeng 16:1277-1284

[136] Youn SW, Takahashi M, Goto H, Maeda R and Kobayashi N (2006) AFM, SEM and Nano/micro-indentation studies of the FIB-milled glassy carbon surface heat-treated at different conditions. In DTIP 2006: April 26-28, 2006, 2006.

[137] Gamero-Castaño M (2008) The structure of electrospray beams in vacuum. J Fluid Mech 604:339-368

[138] Gamero-Castaño M (2008) Characterization of the electrosprays of 1-ethyl-3-methylimidazolium bis(trifluoromethylsulfonyl) imide in vacuum. Phys Fluids 20:032103

[139] Gamero-Castaño M (2002) Electric-field-induced ion evaporation from dielectric liquids. Phys Rev Lett 89:147602

[140] Taylor G (1964) Disintegration of Water Drops in an Electric Field. Roy Soc London Ser A 280:383-397

[141] Chou SY, Krauss PR and Renstrom PJ (1996) Imprint Lithography with 25-Nanometer Resolution. Science 272:85-87

[142] Chou SY, Krauss PR and Renstrom PJ (1995) Imprint of sub-25 nm vias and trenches in polymers. Appl Phys Lett 67:3114-3116

[143] Chou SY, Krauss PR, Zhang W, Guo L and Zhuang L (1997) Sub-10 nm imprint lithography and applications. J Vac Sci Technol B 15:2897-2904

[144] Lal Das A, Mukherjee R, Katiyer V, Kulkarni M, Ghatak A and Sharma A (2007) Generation of Sub-micrometer-scale Patterns by Successive Miniaturization Using Hydrogels. Adv Mater 19:1943-1946